FINAL REPORT

Rapid Response Surveys of Mobility, Burial and Re-exposure of Underwater Munitions in Energetic Surf-Zone Environments and Object Monitoring Technology Development

SERDP Project MR-2729

APRIL 2020

Peter Traykovski
Fredric Jaffre
Woods Hole Oceanographic Institution

SERDP
DOD ▪ EPA ▪ DOE

REPORT DOCUMENTATION PAGE

Form Approved
OMB No. 0704-0188

1. REPORT DATE *(DD-MM-YYYY)*	**2. REPORT TYPE**	**3. DATES COVERED** *(From - To)*
28/04/2020	SERDP Final Report	6/23/2017-6/22/2020

4. TITLE AND SUBTITLE

Rapid Response Surveys of Mobility, Burial and Re-exposure of Underwater Munitions in Energetic Surf-Zone Environments and Object Monitoring Technology Development
MR-2729 Final Report

5a. CONTRACT NUMBER

5b. GRANT NUMBER
#W912HQ17C0012

5c. PROGRAM ELEMENT NUMBER
MR-2729

6. AUTHOR(S)
Peter Traykovski and Fredric Jaffre

5d. PROJECT NUMBER
49001201

5e. TASK NUMBER

5f. WORK UNIT NUMBER

7. PERFORMING ORGANIZATION NAME(S) AND ADDRESS(ES)

Woods Hole Oceanographic Institution
266 Woods Hole Rd
Woods Hole, MA 02540

8. PERFORMING ORGANIZATION REPORT NUMBER
MR-2729

9. SPONSORING / MONITORING AGENCY NAME(S) AND ADDRESS(ES)
Strategic Environmental Research and Development Program
4800 Mark Center Drive, Suite 16F16
Alexandria, VA 22350-3605

10. SPONSOR/MONITOR'S ACRONYM(S)
SERDP

11. SPONSOR/MONITOR'S REPORT NUMBER(S)
MR-2729

12. DISTRIBUTION / AVAILABILITY STATEMENT
DISTRIBUTION STATEMENT A. Approved for public release: distribution unlimited.

13. SUPPLEMENTARY NOTES

14. ABSTRACT

The development of predictive models and measurement techniques for the mobility, burial and re-exposure of munitions is essential to planning remediation efforts. The goal of the this work was to develop technology for rapid response surveys of seafloor morphology, bathymetry, location and state of burial of surrogate UXO and conduct field measurements that span the relevant parameter space at the transition from burial to initial mobility and to migration. To further our understanding of UXO burial and mobility processes, realistic size and density active UXO surrogates were deployed in the surf-zone immediately before extremely energetic wave events. This rapid response mode of deployment surveying aimed to fill gaps in our knowledge in parts of parameter space (very energetic conditions, rapidly changing bathymetry and realistic UXO densities) that have not been adequately sampled by previous field efforts. The location of the UXO and surf-zone bathymetry was surveyed using a recently developed small autonomous surf capable vessel (ASV) with a PPK GPS/Echosounder bathymetry sensor and ultra-short base line (USBL) receiving array for tracking surrogate UXO with active acoustic sources. This study documented that hydrodynamic sand sediment transport convergence associated with sand bar dynamics (e.g. the balance between offshore directed undertow and onshore directed wave skewness and acceleration) can result in little UXO migration even in very energetic surf zone conditions, in contrast to a previous study which had large migration rates in moderate conditions. The parameterized dynamic force balance model was used to successfully hindcast UXO migration using forcing from the SWASH nearshore wave and flow model. These deterministic models have potential to be used as input to statistical models for operation over longer time periods and larger spatial domains with greater uncertainty in forcing conditions.

15. SUBJECT TERMS
Munitions Response, Nearshore Hydrodynamics, Sediment Transport

16. SECURITY CLASSIFICATION OF:			**17. LIMITATION OF ABSTRACT**	**18. NUMBER OF PAGES**	**19a. NAME OF RESPONSIBLE PERSON**
					Peter Traykovski
a. REPORT Unclassified	**b. ABSTRACT** Unclassified	**c. THIS PAGE** Unclassified	UU	42	**19b. TELEPHONE NUMBER** *(include area code)* *508-289-2638*

Table of Contents

List of Figures 3
Acronyms 5
Abstract 6
1. Objectives 8
1.1. SERDP Relevance 8
2. Background 8
2.1. Theory 10
2.1.1. Object Mobility 10
2.1.2. Object Burial 12
2.2. Previous Measurements and analysis 13
3. Materials and Methods 15
3.1. Location Study Sites 15
3.2. UXO Surrogate Objects 16
3.2.1. SUXO Active Pingers 17
3.2.2. Embedded Motion, Pressure and Light Sensors 17
3.3. Autonomous Surface Vessel Based Bathymetric Mapping and sUXO Tracking Techniques 18
3.3.1. Bathymetric Sensors and Processing 19
3.3.2. Long Point Surf Zone Bathymetry 20
3.3.3. Combined Doppler and USBL based sUXO Tracking 22
3.4. Measurement Techniques for Forcing Hydrodynamics 26
4. Results and Discussion 27
4.1. Hydrodynamic forcing 27
4.1.1. Offshore Wave Measurements 27
4.1.2. Sand Bar Migration 29
4.1.3. sUXO Surrogate Deployments, large scale mobility and burial 31
4.2. Numerical Modeling of sUXO Migration 33
5. Conclusions and Implications for Future Research/Implementation 35
6. Literature Cited 37
7. Appendices 38

List of Figures

Figure 1. Migration trajectories of sUXO deployed in the surf-zone off Long Point, Martha's Vineyard, MA measured with both USBL based tracking (dashed lines) and small buoy GPS surveys (solid lines) overlaid on bathymetric data taken with the Jetyak and a backpack GPS survey on the subaerial beach. Colored lines are $L = 0.75$, $D_0 = 0.15$ m objects and yellow lines are $L = 0.75$, $D_0 = 0.07$ m objects. 9
Figure 2. UXO Surrogate Migration as a function of Depth and Relative Density (S). Colored lines represent start and end depths of object that migrated and red dots indicate objects that buried and did not migrate. The relative density separates objects into regimes that bury $\rho 0 \rho water > 3$, a transitional regime $2 < \rho 0 \rho water < 3$, and a mobile regime $\rho U 0 \rho water < 2$ 10
Figure 3. Schematic of torque balance on a cylinder 11
Figure 4. Threshold for initiation of motion as a function of UXO density and wave forcing for the RBF16 emprically tuned parameterization and Eqns 1&2. 13
Figure 5 (a) Threshold for initiation of UXO motion as a function of U_{br} and S_o based on asumed initial fractional burial of 10% and 30%. (b) Threshold for initiation of motion based on an equilibrium burial depth assumption. 14
Figure 6. Threshold for initiation of UXO for the time depedent burial calcuations coupled to the phase resolved mobility model. a) dU_{br}/dt =1 m/s/hr, b) dU_{br}/dt =0.5 m/s/hr, c) dU_{br}/dt =2 m/s/hr. 15
Figure 7. Location of study site and Cape Cod regional bathymetry, with aerial imagery of Wasque Shoals, and sidescan sonar imagery of the area near Martha's Vineyard Coastal Observatory (MVCO) 16
Figure 8. MVCO wave height statistics 17
Figure 9. Surrogate UXO. The light and pressure sensor can been seen on the near end of the sUXO and the the tether and small buoy on the far end. 18
Figure 10. Surf-Zone Capable Autonoumous Surface Vessel A) Surveying in calm condtions at the field site. B) Jet Drive. C) USBL Array and Single Beam Echosounder Transducer. D) CAD Model of the hull with theself rigthting flotation lid. E) Stabilty results from CAD model 19
Figure 11. Long Point surf zone site bathymetry A) 9/4/2014. B) 10/26/2018 20
Figure 12. Google Earth Imagery of Long Point A) 12/30/2010, B) 5/10/2016 C) 4/14/2017 D) 10/05/2018 . Red boxes Indicate areas surveyed in 2014 and 2018 shown in Figure 11. 21
Figure 13. Doppler shift of the pings received on the USBL array. The color represents the magnitude of yd, an the red line is a time series of the peak of the Doppler spectra. A) Entire Survey, B) From 750 to 850 seconds as the ASV passes the target emitting at 34 kHz. c) Doppler Shift Spectra for 5 pings near the target (t=771 to 775 s) and average of the 5 pings (thick red line) plotted vs Doppler Shift Frequency (f_d) The angular coordinates transformed from Doppler Shift Via Eqn 25 is shown above the plot on the upper x-axis. Predicted Spectra from frequency domain theory is shown as a black dotted line. All spectra are shifted to have peaks at $f_d = 0$. Lower Panel: Doppler Shift Beam patterns for 5 pings near the target (t=771 to 775 s) and average of the 5 pings (thick red line) spatial domain theory is shown as a black dotted line} . 23
Figure 14. Beamforming of the pings received on the USBL array after Doppler compensation. The color represents the magnitude of yb, and the red line is a time series of the peak of the beamformer angular spectra. A) Entire Survey, B) From 650 to 850 seconds as the ASV passes the target emitting at 34 kHz. C) USBL Beam Pattern for 5 pings near the target (t=771 to 775 s)

and average of the 5 pings (thick red line). Predicted Beam Pattern from theory is shown as a black dotted line. All Beam Patterns are shifted to have peaks at q_s = 90. 24
Figure 15 A) Gridded Doppler beam pattern for an individual ping near one of the Targets. B) Sum of all gridded Doppler beam pattern with a blue marker at the location of the target estimated by the peak of the sum. C) Sum of all gridded USBL beam pattern with a blue marker at the location of the target estimated by the peak of the sum from the Doppler estimates and a cyan marker for the USBL estimates. 25
Figure 16. Results of gridded tracking from GPS Buoys (Red stars), Combined Doppler and Beamforming (Black Dots), Beamforming Only (Green Stars), Doppler Only (Blue Stars). The targets are labelled by pinger frequency in kHz. 26
Figure 17. A) Wave Height (Hm0) from the Spotter Buoy, CDIP Buoy and CDIP data scaled by 0.6. B) Mean (blue line) and Peak (green line) Wave Period from the Spotter buoy and CDIP buoy (red line). C) Wave direction with the same lines types as B. 27
Figure 18. Wave measurements inside the surf zone from the Vector ADV located in 2 m water depth. A) Depth, B) Wave Height, C) Wave Orbital Velocity, and D) Skewness and Acceleration. 28
Figure 19. Measurements from the TCMPs with ADV data for reference. A) Eastward mean flows, B) Northward Mean Flows, C) Wave Height from pressure, and D) Water Depth from pressure. 29
Figure 20. Topo-Bathymetry measurements with elevation relative to NAVD88. A-C) Topo-Bathymetric surfaces from the three surveys with 1 m spaced contours (solid lines), 0.5 m contours (dashed lines), and the red line indicates the z=0 contour level. D) Cross-Shore Transects from X= -40 mS(solid) ,0 m (dotted) and 40 m (dashed) for the three surveys. 30
Figure 21. Topo-Bathymetry elevation difference (ΔZ) measurements for the 10/31 – 10/26 surveys. A) Difference map with red indicated deposition, and red erosion. B) Transects of ΔZ at X= -40 mS(solid) ,0 m (dotted) and 40 m (dashed) 30
Figure 22. sUXO and instrument deployment (Green *) and final locations if migration occurred (Yellow *) on A) Topo-Bathymetry maps and B) elevation difference (ΔZ) maps 31
Figure 23. A) Tide resovling Low Pass Filtered (L.P.F-dashed lines) and sliding window RMS pressure from each sUXO. B) Presssure relative to a reference from the ADV sesnor on a fixed pole mount, + indicates the sUXO becoming shallower than the reference. C) Roll and D) Light from the sUXO embedded sensors. At solid balck line indicates Oct 27, 14:00 hours at the minimum of relative pressure. 32
Figure 24. A) Temporal snapshot of cross-shore velocity output from the SWASH model. B-D) SWASH model results for a range of input wave heights color coded from blue with *Hs* = 1 m to red with *Hs*=3.5 m. The blue and red dashed line represents the offshore extent of the surf zone and the approximate balance point between onshore and offshore directed forcing for small waves and large wave respectively. 33
Figure 25. Results of the UXO migration model forced by SWASH hydrodynamics output for 2014/2018 MV experiments with large input waves (*Hs*=4.0 m) representing 2018 and smaller waves representing (*Hs* = 2.5 m) 2014. A) sUXO trajectories, B) SWASH model input bathymetry 34

Acronyms

ADV	Acoustic Doppler Velocimeter
AUV	Autonomous Underwater Vehicle
ASV	Autonomous Surface Vessel
CAD	Computer Aided Design
CDIP	Coastal Data Information Program
CONUS	Contiguous United States
CORS	Continuously Operating Reference Station
EKF	Extended Kalman Filter
ESTCP	Environmental Security Technology Certification Program
FY	Fiscal Year
GPS	Global Positioning System
IMU	Inertial Motion Unit
MATPL	Magnetic, Acceleration, Temperature, Pressure, Light
MRLA	Minimum Redundancy Linear Array
MRSON	Munitions Response Statement of Need
MVCO	Martha's Vineyard Coastal Observatory
NAD	North American Datum
NAVD	North American Vertical Datum
PC	Personal Computer
PPK	Post-Processed Kinetic
PVC	Polyvinyl Chloride
SERDP	Strategic Environmental Research and Development Program
SNR	Signal-to-Noise Ratio
sUXO	surrogate UXO
SWASH	Simulating WAves till SHore
TCMP	Tilt Current Magnetic Pressure
UAV	Unmanned Aerial Vehicle
UnMES	Underwater Munitions Expert System
USACE	United States Army Corps of Engineers
USBL	Ultra-Short Base Line
UXO	Unexploded Ordnance
WHOI	Woods Hole Oceanographic Institution

Abstract

Objectives: The development of predictive models and measurement techniques for the mobility, burial and re-exposure of munitions is essential to planning remediation efforts. In sandy, energetic near-shore environments, migration, burial and re-exposure processes all have potential to be active depending on the munition properties and forcing parameters. The goal of this work is to develop technology for rapid response surveys of seafloor morphology, bathymetry, location and state of burial of surrogate UXO (with imbedded acoustic sources) and conduct field measurements that span the relevant parameter space at the transition from burial to initial mobility and to migration. In order to further our understanding of UXO burial and mobility processes, realistic size and density active UXO surrogates will be deployed in the surf-zone immediately before extremely energetic wave events. This rapid response mode of deployment surveying will fill gaps in our knowledge in parts of parameter space (very energetic conditions, rapidly changing bathymetry and realistic UXO densities) that have not been adequately sampled by previous field efforts.

Technical approach: The analysis is guided by a parameterized dynamic force balance model for the mobility and burial of UXO in sandy sediments. The parameterizations of the roles of relative object density and hydrodynamic drag due to wave and current forcing on both stationary and mobile objects will be examined with previous measurements and a new set of measurements in the surf zone during very energetic conditions. Conducting measurements of UXO mobility and burial in regions of the surf zone with mobile bathymetry during energetic events is very challenging as the bubbles make the water column acoustically opaque and the migrating sand bars tend to bury sensors and UXO. In addition, surrogate UXO deployed in moderately energetic conditions will often bury before a subsequent very energetic event which would have caused mobility. To account for this, we deployed surrogate UXO in a rapid response mode immediately before a large event. The location of the UXO and surf-zone bathymetry was surveyed using a recently developed small autonomous surf capable vessel (ASV) with a PPK GPS/Echosounder bathymetry sensor and ultra-short base line (USBL) receiving array for tracking surrogate UXO with active acoustic sources ("pingers"). A new tracking methodology was developed that relies on the Doppler shift of the received signal and the GPS measured vessel motion to localize the pingers. This avoids the use of expensive USBL technology. The use of commercially available pingers will allow this methodology to be easily extended to a larger community for future projects. The surrogate UXO contained a new generation of low power / long endurance internal sensors to monitor waves, currents, orientation and state of burial.

Benefits: The measurements conducted in this study provided a unique data set on munitions burial and migration in more energetic nearshore conditions than our previous studies where the potential for significant migration is high. In particular, this study documented that hydrodynamic sand sediment transport convergence associated with sand bar dynamics (e.g. the balance between offshore directed undertow and onshore directed wave skewness and acceleration) can result in little UXO migration even in very energetic surf zone conditions. The parameterized dynamic force balance model was used to successfully hindcast UXO migration using hydrodynamic forcing from the SWASH nearshore wave and flow model. These deterministic models have potential to be used as input to statistical models for operation over longer time periods and larger spatial domains with greater uncertainty in forcing conditions.

1. Objectives

The development of predictive models for the mobility, burial, and reexposure of munitions is essential to planning remediation efforts. In sandy, energetic nearshore environments, the migration, burial and reexposure processes all have the potential to be active depending on the munition properties and forcing parameters. The parameter space in which objects migrate significant distances has not been thoroughly examined with quantitative field measurements. To obtain data to quantify these processes and test models, we conducted field measurements of mobility, burial, and reexposure of munitions in energetic nearshore environments with a high potential for mobility. The surrogate munition's type, size, and density were varied to enhance the potential for migration processes. This study follows from a successful study with similar goals conducted in 2014 (MR-2319 [1]), where low density surrogate UXO ($\rho_0 < 2.5$ g/, and henceforth referred to as sUXO) were observed to migrate up to 160 m across the surf zone, and denser objects buried in place in response to waves with 2.5 m significant wave height (H_s). One of the specific objectives of this study was deploy sUXO in rapid response mode before very energetic storms to determine if denser UXO would also migrate during more energetic conditions as most actual UXO are denser than ρ_0 of 3.5 g/cm^3. New technology to more efficiently measure the mobility and burial of sUXO was developed during the study, including a new suite of embedded sensors and autonomous surface vessel (ASV) based tracking methods. A small surf capable ASV was developed to house the trackers and to perform bathymetric surveys in the surf zone. The measurements were examined to understand munition mobility and burial processes, as well as to develop relations between these processes and hydrodynamic forcing. Finally, simple parameterized models were examined and refined in the parameter space consistent with the observations. In MR-2319 these models quantified the thresholds for mobility as function of hydrodynamic forcing and object characteristics but did not describe migration rates or distances. The modelling objectives of the current study included updates to account for dynamic UXO objects and can now be used for quantifying object migration rate and distances. The simple parametrized models were coupled to the output of a numerical hydrodynamics and wave model (SWASH) to account for gradients and convergences in wave and current forcing in migration predictions.

1.1. **SERDP Relevance**

One of the areas outlined in the SERDP munitions response program area FY 2017 statement of need (MRSON 17-01) was the characteristics of underwater munitions and their environment. This includes "Assessing the environment in which the munitions are found. Characteristics such as sediment type, seafloor morphology, hydrodynamic conditions, and water column turbidity or visibility may impact the detection and characterization of munitions underwater" and "Assessing the relative abundance of intact munitions, munitions-related debris (including fragments, scrap, and remains of targets), and other sources of clutter at multiple sites." While the environmental assessment issues in the first goal are fairly obvious, the second goal of assessing the abundance of intact or fragmented munitions also requires knowledge of the state of burial or potential for mobility of the objects.

2. Background

Recent field measurements (MR-2319 and MR-2320 [2]) of the mobility, burial and re-exposure of munitions have significantly increased our knowledge of the parameters which control

mobility and burial, and work is underway in developing predictive models based on these parameterizations. However, there are still significant gaps in our knowledge of these processes in certain regimes of parameter space where extensive migration of realistic density UXO is possible.

The measurements in MR-2319 conducted on the South Shore of Martha's Vineyard, MA (Figure 1) indicate that medium sized (D_0 = 7 and 15 cm, L = 75 cm) objects with densities less than 2.5 g/cm^3 migrate distances over 100 m across the surf zone in the onshore direction in moderate wave energy conditions with wave orbital velocities of U_w ~ 70 to 100 cm/s (2.5 m height incoming waves in 3 to 4 m water depth). These measurements represent some of the first well constrained field measurements of sUXO migration over distances greater than 10s of meters, and thus begin to define the parameter regimes of the transition from mobility and burial with in-situ field data.

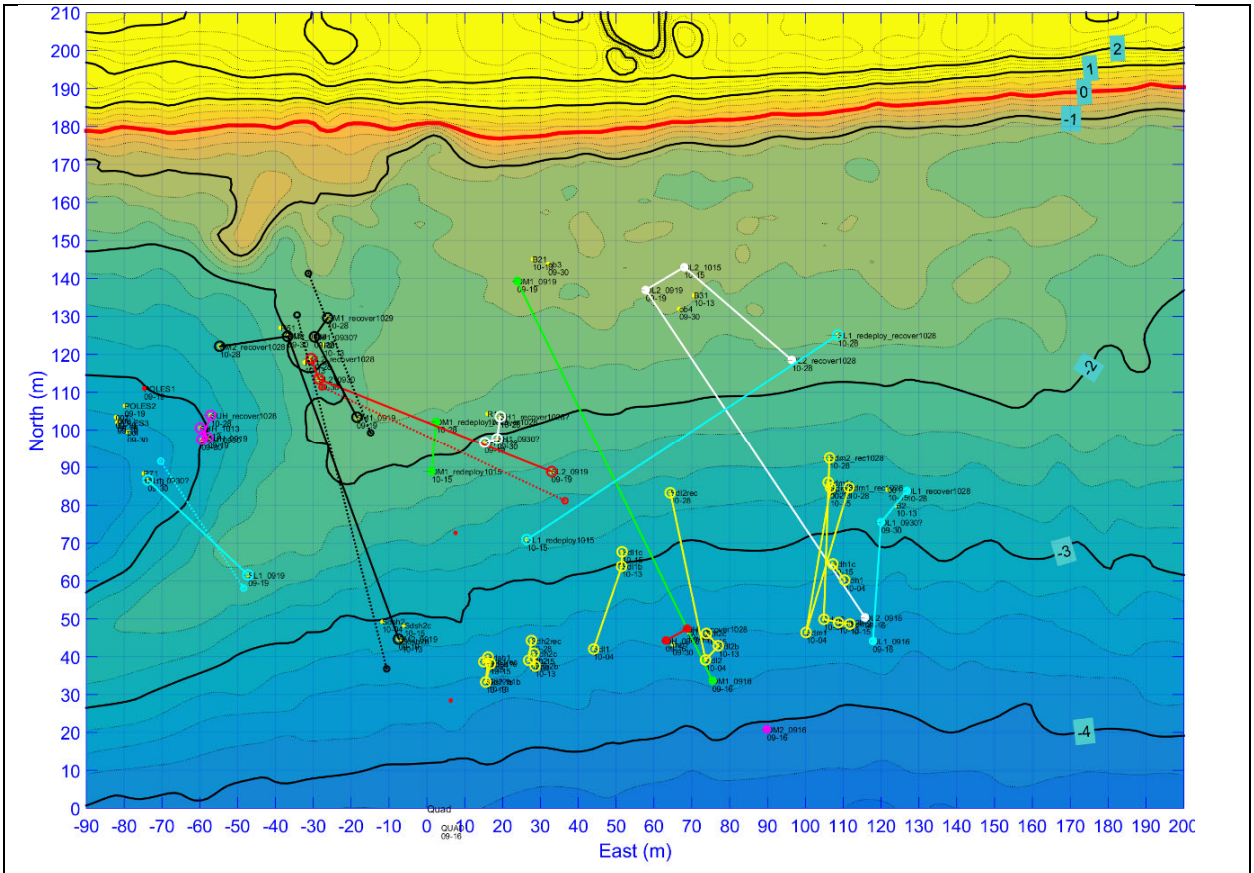

Figure 1. Migration trajectories of sUXO deployed in the surf-zone off Long Point, Martha's Vineyard, MA measured with both USBL based tracking (dashed lines) and small buoy GPS surveys (solid lines) overlaid on bathymetric data taken with the Jetyak and a backpack GPS survey on the subaerial beach. Colored lines are L = 0.75, D_0 = 0.15 m objects and yellow lines are L = 0.75, D_0 = 0.07 m objects.

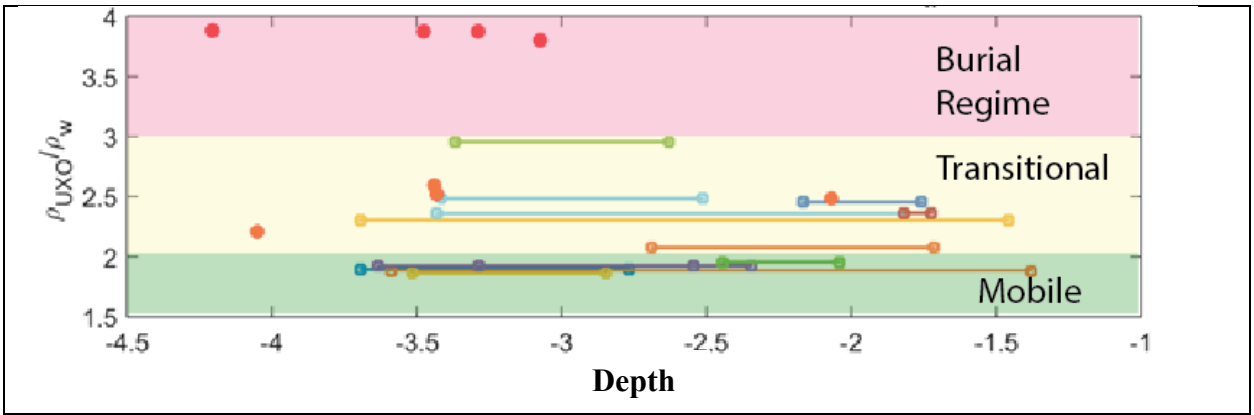

Figure 2. UXO Surrogate Migration as a function of Depth and Relative Density (S). Colored lines represent start and end depths of object that migrated and red dots indicate objects that buried and did not migrate. The relative density separates objects into regimes that bury $\frac{\rho_0}{\rho_{water}} > 3$, a transitional regime $2 < \rho_0/\rho_{water} < 3$, and a mobile regime $\frac{\rho_{U0}}{\rho_{water}} < 2$

The objects at this site were deployed in depths of 3 to 4 m (Figure 2). Objects with densities close to 4 g/cm^3 did not migrate and were buried in place with burial depths up to 50 cm. In MR-2319, the density range between 1.5 and 2.5 g/cm^3 was well sampled with several different density sUXO to ensure that some sUXO would migrate even during moderate wave energy conditions. The region between 2.5 and 4.0 g/cm^3 was not well sampled as there were sUXO at these two end members, but few in-between. Measurements conducted at the USACE Field Research Facility at Duck, NC as part of MR-2320 in 8 m depth water, with 5 m significant wave height (U_w ~ 150 to 180 cm/s) and object densities greater than 2.5 g/cm^3 indicated all objects buried in place. In 8 m water depth, the objects were deployed well offshore of the mobile near-shore sand bars, which formed at 3 to 5 m water depths. However, with 5 m high waves, the measurements were in the outer portion of the surf zone during the most energetic conditions.

The region in the vicinity of the nearshore sand bar also has potential for burial of UXO beyond the 1 to 3 object diameters typically associated with scour burial, as migrating sand bars can bury objects to depths of several meters, making detection by even the most advanced acoustic and electromagnetic sensors challenging. Thus, in addition to measuring UXO mobility, measurements of bathymetric change in the nearshore are essential to understand the potential for deep burial.

2.1. **Theory**

2.1.1. Object Mobility

The parameter space where burial vs. migration is expected can be examined by considering the moments on an object and the grains of sand. In a highly simplified analysis, the moment per unit length that will induce roll of the cylinder is $T_f = FD_0(1/2 - p_b)$, where D_o is the diameter of the object, p_b is the fractional burial and is related to the depth of burial by $p_b = b_d/D_o$. The total lateral force (F) on the object consists of the sum of three terms, the drag force (F_D), the inertial force (F_I) and the pressure gradient force (F_P), $F = F_D + F_I + F_P$. The drag force due to water velocity (U) is $F_D = \rho_w C_d U|U|D_0/2$, the inertial term is $\frac{F_I = C_m \rho_w \pi D_0^2 \dot{U}}{4}$, and the pressure gradient term is $F_P = \rho_w \pi D_0^2 \dot{U}/4$. In these expressions C_d and C_m are drag and added coefficients, and ρ_w is water density. The stabilizing moment caused by the weight of the

cylinder per unit length when the object is less than halfway buried is $T_w = WD_0\sqrt{p_b(1/2 - p_b)}$, based on a submerged weight of $W = g\frac{(\rho_0 - \rho_w)\pi D_0^2}{4}$. The ratio of the destabilizing forces due to drag only and the stabilizing forces is quantified by the object Shields parameter (θ_{op_b}) based on percent burial ($p_b = \frac{b_d}{D}$):

$$\theta_{op_b} = \frac{C_d U|U|^2}{g(S_o - 1)D_0}\frac{2\left(\frac{1}{2} - p_b\right)}{\pi\sqrt{p_b\left(\frac{1}{2} - p_b\right)}} = \theta_o\frac{2\left(\frac{1}{2} - p_b\right)}{\pi\sqrt{p_b\left(\frac{1}{2} - p_b\right)}} \quad (1)$$

The key parameters in this expression are the diameter of the object and the initial depth of burial as these determine the moment arms, and the current velocity (U) combined with the relative density of the object ($S_o = \frac{\rho_0}{\rho_w}$, where ρ_0 is UXO density) as these determine the forces.

A similar analysis on a grain of sand with median diameter d_{50} results in the Shields criteria for initiation of sand motion ([3]). The Shields parameter based on percent burial (θ_{op_b}) can be expressed as the Shields parameter from sediment transport theory θ_o and a geometric term related to initial burial, which is similar to a frictional coefficient. This geometric term only accounts for the geometry of the lever arms in the torque balance and not in the reduction in exposed diameter for the drag term or reduction in area for the inertial and pressure gradient terms due to burial. At low values of p_b the difference is small, but it does become significant as the object becomes buried further.

These calculations are based on the assumption of a stationary object and thus are used to calculate thresholds of initial motion. For a dynamic analysis to calculate migration rate and distance the water velocity can be replaced by the relative velocity between the water and the object (U-U_0). The acceleration of the object can be calculated from a force balance

$$\frac{\rho_0\pi D_0^2\dot{U}_0}{4} = F - \mu W \quad (2)$$

Where the friction coefficient is given by $\mu = \sqrt{p_b\left(\frac{1}{2} - p_b\right)}\Big/\left(\frac{1}{2} - p_b\right)$. These dynamic calculations require the full phase resolved series of water velocity as the shape of the wave is important for correctly calculating the flow acceleration ($\dot{U}_0$). The migration distance of the object can be found by integrating the object acceleration in Eqn (2: $X = \iint \dot{U}_0 dt$.

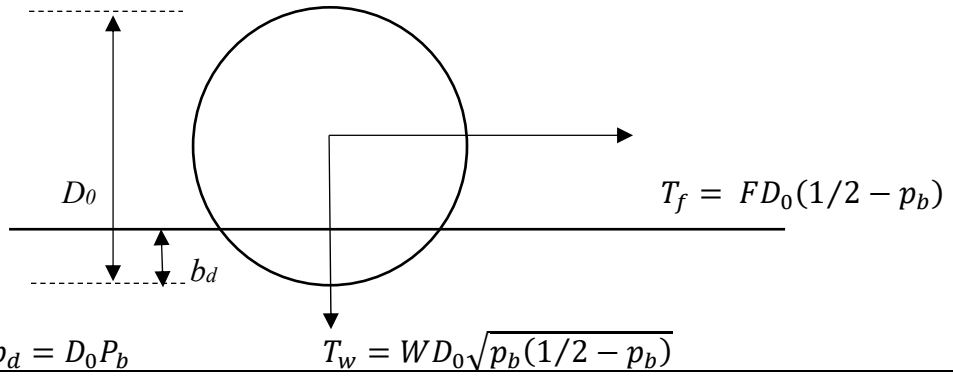

Figure 3. Schematic of torque balance on a cylinder

A recent reanalysis of previously collected data with additional new laboratory data on the initiation of UXO motion was conducted by Rennie, Brandt, and Friedrichs (RBF16, [4]). Based on a similar conceptual framework as discussed above they propose a relationship whereby the object Shields parameter (θ_o) is modified by an inertial term that accounts for the effects of flow acceleration due to waves as

$$f_I = (1 + 16\pi^2 (C_I/C_D)^2 KC^{-2})^{\frac{1}{2}} \tag{3}$$

where C_I/C_D is approximately 2 for cylinders, and the Keulegan–Carpenter number is defined as $KC = \frac{U_{br}T}{D_0}$. The variable U_{br} is the representative nearbed wave orbital velocity, and *T* is the peak wave period. Since a wave averaged approach is used this method can only calculate the mobility threshold and cannot calculate migration rates. Based on a fit to various data sources, RBF16 found a power law relation between the modified Shields parameter and the initial depth of fractional burial (p_b) of the form:

$$f_I \theta_o = 1.64\ (p_b)^{0.71} \tag{4}$$

This criterion for mobility is illustrated as a relation between critical velocity and object relative density (S_o) for several different initial burial depths in Figure 4 and is compared to results from the phase resolved solution described by Eqns 1&2. To align the transition from stationary (red) to mobile (green) from the two approaches the friction parameter was scaled by 0.4. Some of this discrepancy may be due to the fact that the empirical approach is using wave averaged representation of wave forcing (e.g. U_{br}) , and that friction coefficient is more complex than this simple rigid bed model due to deformation of the bed.

2.1.2. Object Burial

Laboratory data and some field data have also been used to develop parameterized expressions for the state of burial of cylinders, mines, and ordnance-shaped objects. There is a large body of literature on this subject and the results are well summarized in RBF16 and a recent publication by Friedrichs, Rennie, and Brandt ([5]). This work suggests the following expression for equilibrium burial depth:

$$p_{b,eq} = a_2 \theta_{sed}^{b_2} \tag{5}$$

The values of Catano-Lopera et al. ([6]) of $a_2 = 1.6$ and $b_2 = 0.85$ for wave periods of T > 4 s were used for predictions of burial depth in this study. The sediment Shields parameter based on sediment relative density $S_{sed} = \rho_{sed}/\rho_0$ is calculated from

$$\theta_{sed} = \frac{f_w U_{br}^2}{g(S_{sed} - 1) d_{50}} \tag{6}$$

where the wave friction factor is based on the expression from Nielsen ([7]), in which d_{50} is the median grain diameter of the sand:

$$f_w = \exp\left(5.5 \left(\frac{12 U_{br} T}{2\pi d_{50}}\right)^{-0.2} - 6.3\right) \tag{7}$$

The equilibrium burial depth formulations relate the final depth of burial to constant wave forcing conditions. The burial process is known to take a finite amount of time, which is related

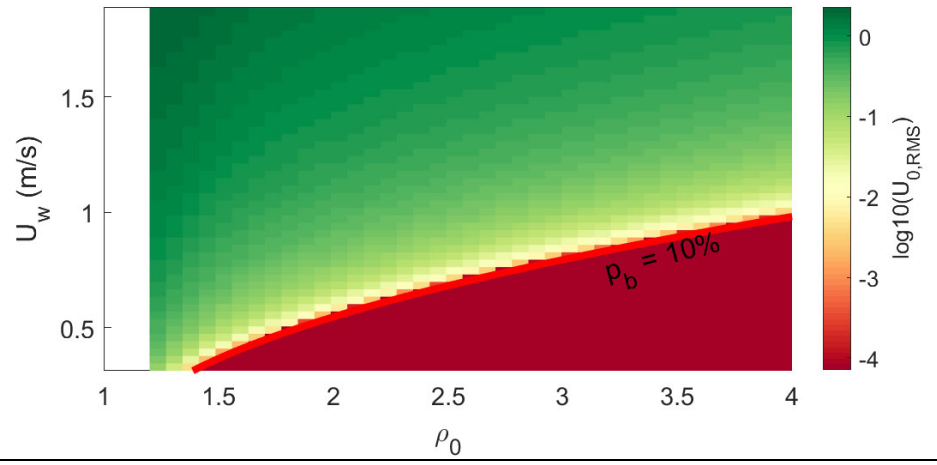

Figure 4. Threshold for initiation of motion as a function of UXO density and wave forcing for the RBF16 emprically tuned parameterization and Eqns 1&2.

to the sediment transport rate and the size of the scour pit that the object will self-bury in. Whitehouse ([8]) modeled time-dependent burial as a logistic process, whereby the burial depth (p_b) follows the equilibrium burial depth ($p_{b,eq}$) with a timescale (T^*):

$$\frac{dp_b}{dt} = \frac{p_{b,eq} - p_b}{T^*} \tag{8}$$

This expression is similar to that used by Traykovski ([9]) for modeling time-dependent evolution ripple geometry. For a step change in forcing, this results in the following:

$$p_b(t) = p_{b,eq}\left(1 - \exp\left(-\frac{t}{T^*}\right)\right) \tag{9}$$

The timescale is the ratio of the object diameter squared to the sediment transport rate:

$$T^* = \frac{\alpha\theta_{sed}^N D_0^2}{(g(S_{sed} - 1)d_{50}^3)^{0.5}} \tag{10}$$

The parameter N is set to 1.5 based on the Meyer-Peter Mueller ([10]) sediment transport rate formulation, and α is used to tune the model to field data sets.

2.2. **Previous Measurements and Analysis**

The mobility thresholds calculated by the RBF16 method and equations 1&2 were compared to measurements of sUXO mobility as described in the MR-2319 final report. When these methods were used to calculate thresholds based on a time invariant burial depth, a single burial depth failed to segregate the data into mobile and non-mobile classes (Figure 5). The model was run with 10% and 30% initial burial. The model predictions are shown as a curve of U_{br} for initiation of motion versus UXO relative density (S_o). Points above the curve are predicted to be mobile (green zone for p_b = 10%), and points below (red zone for p_b = 10%) are predicted to be stationary. The observations are plotted as green points in (U_{br}, S_o) space for mobile objects and red points for stationary objects. Both predictions for p_b of 10% and 30% are inconsistent with

the observations of UXO mobility. A mobility threshold curve based on an initial state of burial of 10% incorrectly predicts that all objects, including those with S_o greater than 2.5, would be

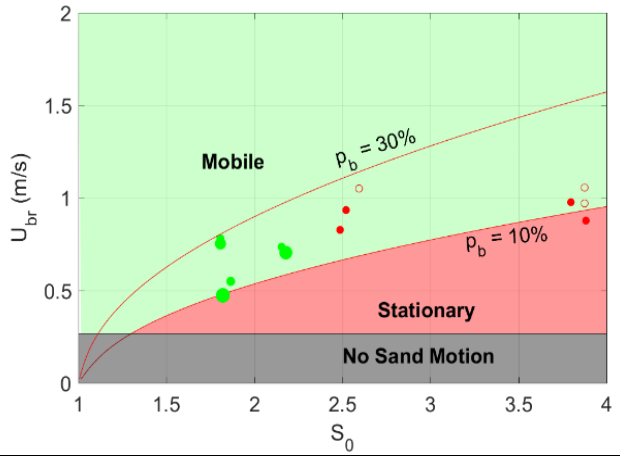

Figure 5 (a) Threshold for initiation of UXO motion as a function of U_{br} and S_o based on asumed initial fractional burial of 10% and 30%. (b) Threshold for initiation of motion based on an equilibrium burial depth assumption.

mobile. A threshold curve based on an initial state of burial of 30% incorrectly predicts that all objects, including those with S_o less than 2.5, would be stationary. Curves between 10% and 30% do not result in better predictions because the theory does not account for the dramatic change in mobility/burial behavior near a relative density of 2.2 to 2.6, which is slightly above the typical density of 2.0 for water-saturated sand beds.

As described in the MR-2319 final report, because the burial process is known to be a time-dependent process, it is not physically realistic to assume a constant initial burial of some predetermined value. The threshold for mobility of objects on a mobile bed is likely to be set by the rate of burial relative to the rate of wave energy increase. If an initially proud object is instantaneously subjected to wave forcing greater than the threshold of motion, it will move before it has time to bury. If the wave forcing is increased very slowly with rates much slower than the timescale for burial, the object will become sufficiently buried with a burial depth given by the equilibrium burial depth (Eqn. 6), so it will not move unless the entire bed is fluidized, which requires extremely high wave energy or strong pressure gradients. In the MR-2319 final report, a method is described that couples the RBF16 wave averaged mobility thresholds with the time dependent burial equations. In the new work, we have coupled the wave averaged burial model with the wave phased resolved mobility model that allows predictions of both mobility thresholds and migration rates. The results of this model are similar to those presented in figure 34 of the MR-2319 final report.

These time-dependent mobility curves show very different behavior than either the fixed burial depth curves or the equilibrium burial depth curves. Initially, when the waves are small, the mobility threshold curve follows the curve based on the initial burial of 10% (Figure 6). Depending on dU_{br}/dt, at some later time, the objects rapidly bury and are no longer mobile. For increasing values of dU_{br}/dt, this occurs at higher values of S_o. The time-dependent mobility predictions with a dU_{br}/dt = 1 m/s/hr successfully segregate the data into mobile and stationary categories, roughly consistent with the data, although some of the points are very close to the

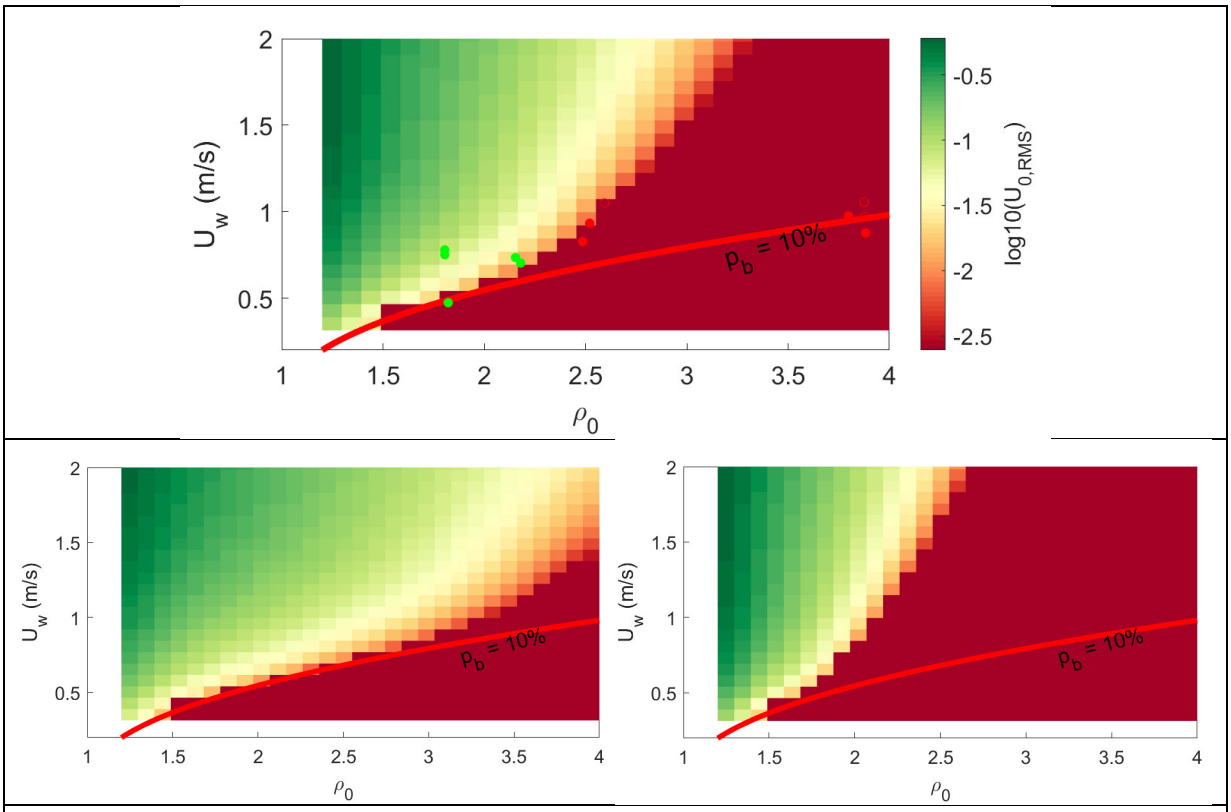

Figure 6. Threshold for initiation of UXO for the time dependent burial calcuations coupled to the phase resolved mobility model. a) dU_{br}/dt =1 m/s/hr, b) dU_{br}/dt =0.5 m/s/hr, c) dU_{br}/dt =2 m/s/hr.

threshold. To segregate the data successfully, the parameter α in the sediment transport rate formulation for the burial timescale was set at 1.1. Comparison of the model migration distance predictions to data from 2014 and 2018 measurements will be discussed in a later section.

3. Materials and Methods

3.1. **Location Study Sites**

The study sites were chosen off the coast of Martha's Vineyard, Massachusetts to allow rapid response to large storms from Woods Hole, MA (Figure 7). In 2013 and 2014 two study sites were used to examine the differences between an environment with strong tidal currents and an energetic surf zone (7). The surf zone measurements in 2014 and 2018 were conducted at the Long Point Wildlife Refuge. Also referred to as the Tisbury Great Pond site, it served as a training range from 1943 to 1947 and has been the subject of remediation efforts. Tidal currents are weak (0.3 m/s in the shore parallel direction) at this site compared to Wasque Shoals, but there is no shallow water offshore, so waves typically break within 1 km of the shoreline with little energy loss offshore due to breaking.

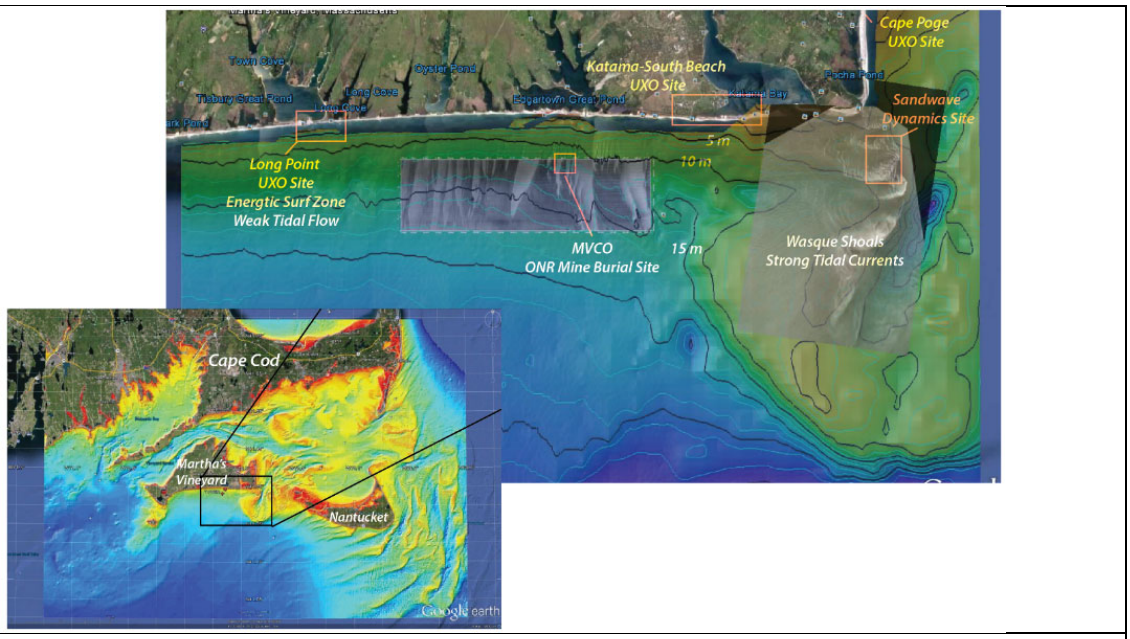

Figure 7. Location of study site and Cape Cod regional bathymetry, with aerial imagery of Wasque Shoals, and sidescan sonar imagery of the area near Martha's Vineyard Coastal Observatory (MVCO)

Based on 15 years of wave height statistics from the Martha's Vineyard Coastal Observatory (MVCO), waves are largest in the winter months (Nov.–March) except for rare hurricanes in the early fall (Figure 8). Thus, the window for rapid response operations was September through December after which low temperatures make diving-based operations difficult. Based on the 10 day sliding window, statistics over 15 years with wave height over 3 m typically occur in less than 5% of the observations thus requiring a rapid response mode of operation using NWS weather and wave forecasting resources.

3.2. **UXO Surrogate Objects**

To measure UXO mobility and burial, a series of sUXO objects were developed with internal motion sensors, acoustic tracking transponders, and both GPS and passive surface buoys. Due to the location of our field measurement sites at land trust and wildlife refuges, which had been used as former training ranges and are now undergoing remediation efforts ([11]), the sUXO could not resemble actual UXO. For this reason, pointed nose sections and tail fins were not used, and a geometry of a straight cylinder was selected. The details of the exact specifications of each sUXO are provided in Appendix A, but they were generally divided into two small (S) diameters (D_0 = 7 cm) and large (L) diameters (D_0 = 14 cm), and four different density classes (very light (VL): S_0 = 2.25, light (L): S_0 =2.5 , medium (M): S_0 =2.75, and heavy (H): S_0 =3.0). The length of the objects for both diameters was fixed at 75 cm. A coding system was used with the first letter for the diameter of the object, the 2nd letter for the density, and A or B at the end to designate the series as two replicates of each geometry before deployment (Table 1). The objects were fabricated from 0.25-inch wall-thickness grade 316 stainless pipe, with PVC endcaps and a mixture of concrete and lead ballasting to achieve the desired density (Figure 9).

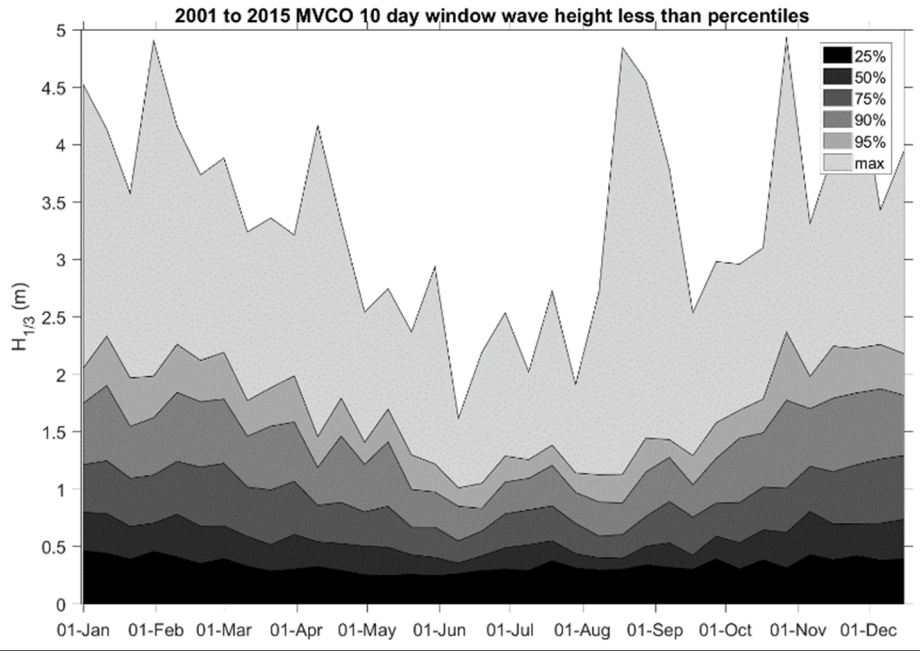

Figure 8. MVCO wave height statistics

3.2.1. sUXO Active Pingers

To track the objects, a Sonotronics active acoustic pinger was attached to 11 of the objects on a 1 m long, 3 mm diameter spectra line, with small (2 cm diameter, by 10 cm long) low drag subsurface float. An additional 4 m of line was connected above the subsurface float to surface buoy with similar dimensions that were used for manual GPS tracking and sUXO recovery. The buoyancy of these floats is 1 % of the lowest density small diameter sUXO and 0.1% of the densest larger diameter sUXO. The projected area ratios and volume ratios of the buoys to the objects are typically less than 3% and 1%, thus the drag and inertial terms are expected to scale accordingly. The pingers transmitted $\tau = 50$ ms duration pulses once per second on individual frequencies from 30 to 40 kHz with 1 kHz separation so that objects could be identified by the frequency.

3.2.2. Embedded Motion, Pressure and Light Sensors

In the 2014 MR-2319 study, an X-IO Inertial Motion Unit (IMU) logger with gyroscopes, accelerometers and magnetometers was embedded in the large diameter objects. The 10 cm diameter of battery pack required for sufficient endurance of the sensor due to the power draw of the gyroscopes only allowed the IMU to be deployed in the larger diameter objects. In 2018 we collaborated with Lowell Engineering to develop the MATPL logger with a 3-axis magnetometer, 3-axis accelerometer, 10 dbar rated pressure sensor and optode passive light sensor. All sensors were logged at 8 Hz, and a single 1.2 cm diameter by 6 cm long lithium battery could power the system for several months. The sensors and logging electronics fit inside a 2.5 cm diameter by 25 cm long pressure case with the light sensor and pressure sensor extending out the end of the sUXO (Figure 9). The accelerometers and magnetometers measured the initiation of motion with the same time reference as the pressure measurements while measuring the durations of rolling and sliding motions along the seafloor. The light sensors measured burial by the absence of light during daylight hours ([12])

Figure 9. Surrogate UXO. The light and pressure sensor can been seen on the near end of the sUXO and the tether and small buoy on the far end.

3.3. **Autonomous Surface Vessel Based Bathymetric Mapping and sUXO Tracking Techniques**

One of the most important measurements for any study of sUXO mobility is bathymetry. In 2014 to measure bathymetry, we used the Jetyak (Jet drive kayak hull) autonomous surface vessel recently developed at WHOI. This hybrid remote control (RC) autonomous surface vessel (ASV) is capable of following GPS waypoint tracks with an accuracy of ±5 m, even in energetic tidal flow conditions, and can operate in 0.5 to 1 m breaking waves in the surf zone. However, the large size (3.5 m length) and weight (150 Kg), make deploying this vessel in surf zone areas difficult and the gas engine is prone to failure due to water entering the air intake. For the 2018 measurements, a smaller (1.8 m long, 15 kg weight) fully sealed electric powered jet drive ASV was developed (Figure 10). The jet drive minimized consequences of running aground and proved safe during launch and recovery operations in the surf. The hull was based on a commercially available (https://shop.centralrcmarine.com/70-CRC-SV40-3.htm) 1/7 scale model of a SV-40 "Outer-Limits" offshore racing hull. The V-shaped hull was cut out in the last 10 in to insert a flat section for mounting the commercially available jet drive (Jet-52 from MHZ jet drives). A digital servo was connected to the steering nozzle with a 3 mm stainless rod that passed through an oil filled fitting for water sealing. An MHZ-Scorpion HK-5035 5.8 kW rated brushless outrunner motor was used to power the jet drive. A Hifei Swordfish Pro+ II 240 Amp electronic speed controller was used to power the motor from two parallel 400 Watt-Hr lithium polymer battery packs in a 6S (22.2V) configuration. This configuration allows rapid acceleration and top speeds of 10 m/s to quickly get measurements in the high impact breaking wave region of the surf zone. Both the motor and speed controller were water cooled with seawater via a constant flow self-priming pump. The original flat lid of the hull was replaced with a rounded floatation module that ensured self-righting stability in the event of a capsize in the surf-zone. The flotation module was designed in Rhino-ORCA CAD software using a model of the boat developed with COTS photogrammetry software (AGISoft Metashape[13]) . Similar to the Jetyak, the vessel was controlled by a pixhawk Cube Ardupilot autopilot which allows rapid transfer from remote controlled modes to GPS waypoint following autonomous modes. In addition to the autopilot computer, a second small form factor single board computer (LattePanda DFR0470-ENT) was used for sensor data acquisition. The data computer ran the Windows 10 operating system to take advantage of software from the sensor manufacturers.

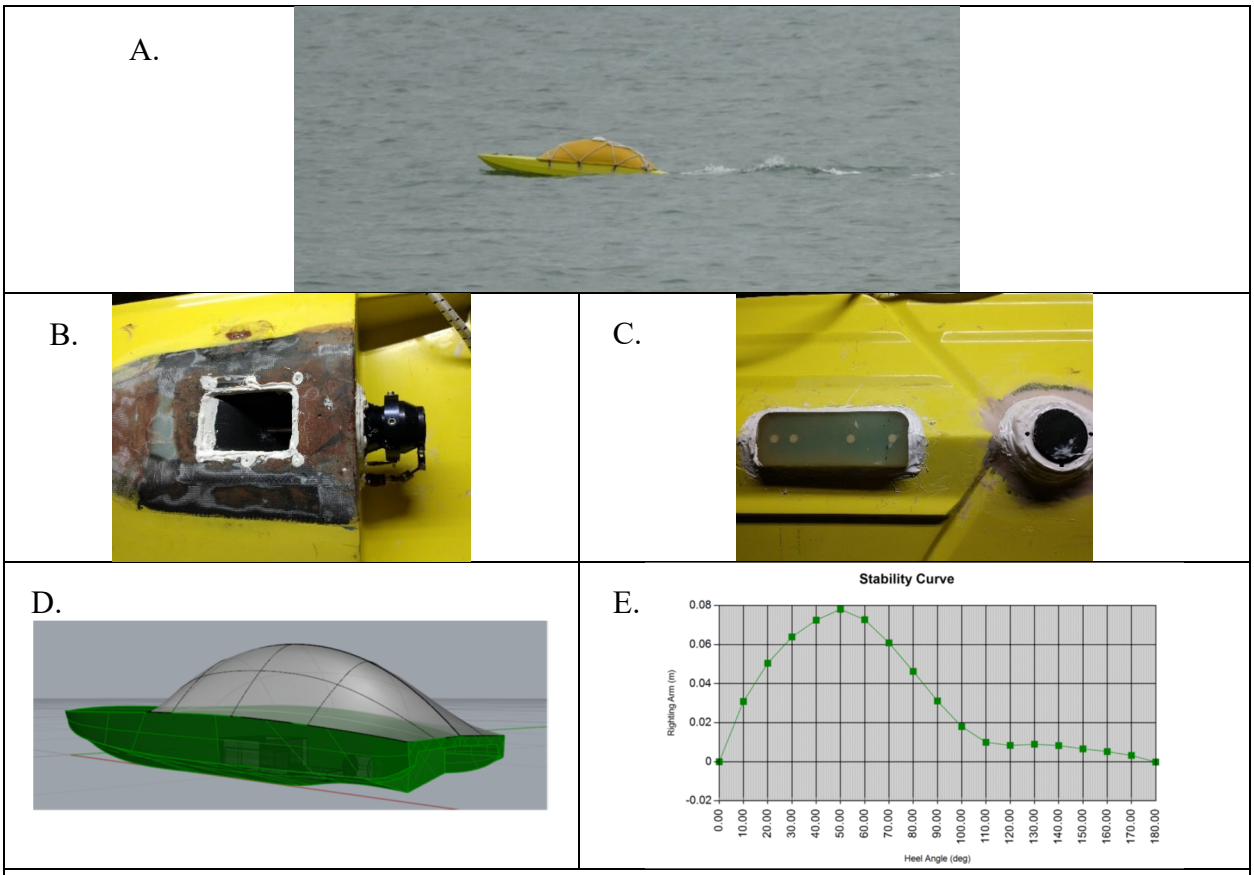

Figure 10. Surf-Zone Capable Autonomous Surface Vessel A) Surveying in calm condtions at the field site. B) Jet Drive. C) USBL Array and Single Beam Echosounder Transducer. D) CAD Model of the hull with the self-righting flotation lid. E) Stabilty results from CAD model

3.3.1. Bathymetric Sensors and Processing

A Javad phase resolving TRE-G3T GPS receiver and L1/L2 AirAnt low profile waterproof Antenna was used for 2 to 3 cm accurate positioning and several mm/s accuracy velocity measurements. The data from this system was recorded internally on the receiver but could be viewed and downloaded to the LattePanda data acquisition computer. Distance from the hull to the seafloor was measured using a dual (200/450 kHz) frequency single beam echosounder (Echologger Dual ECS D24s) with serial communication to the data acquisition computer for real time data visualization and recording. The sonar records the full intensity profile with 7.5 mm range and automatically controlled sampling intervals depending on the distance to the seafloor. The mean sampling rate was 2 Hz.

Bathymetry was processed using a combination of the 450 kHz downward-aimed echo sounder and the Post-Processed Kinetic (PPK) GPS system to resolve both horizontal and vertical positions within several centimeters (2–3 cm horizontal, 3–5 cm vertical). GPS positions were sampled at 10 Hz to accurately capture the vessel position while moving at 2 m/s and to capture the heave motions as the vehicle's vertical position is undulated by waves and tides. The GPS measurements were referenced to a Continuously Operating Reference Station (CORS) in Falmouth, Massachusetts (MAFA), allowing the bathymetry measurement relative to the well-

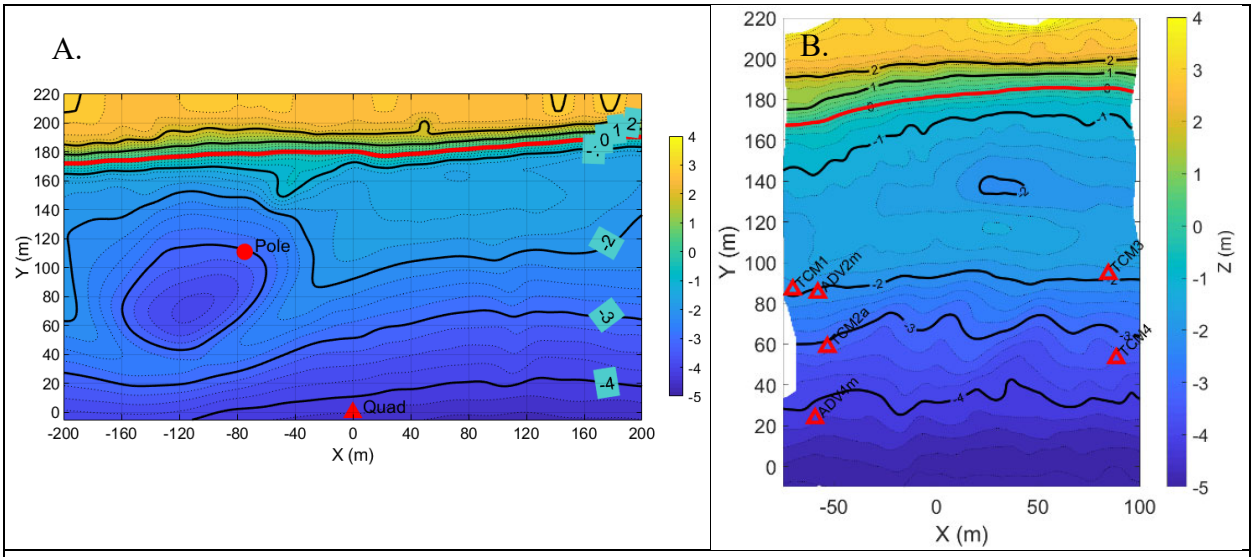

Figure 11. Long Point surf zone site bathymetry A) 9/4/2014. B) 10/26/2018

defined NAD83 datum using the CONUS 12A geiod and NAVD88 vertical datum. In addition to bathymetry measurements at the Long Point surf zone site, beach topography was measured using a PPK GPS backpack system. A walking survey from the base of the foreshore dunes to 1 m water depth was performed at low tide and overlapped with the Jetyak bathymetry surveys performed at high tide. The combined bathymetric and topographic surfaces will be referred to as topo-bathymetric surfaces. Comparison of the three bathymetric surveys on 10/26/2018, 10/31/2018 and 11/05/2018 are discussed in section 4.1.2 as sand bar locations evolve during the storm cycles.

3.3.2. Long Point Surf Zone Bathymetry

The bathymetric and topographic surveys conducted at Long Point reveal a complex nearshore environment with substantial changes on the storm and seasonal time scales. In 2014, an approximately 100 m wide and 1.5 m deep shelf or terrace was present in some locations and 3 m deep holes centered 100 m from the beach were present in other locations (Figure 11). In 2018, based on the first survey the topography appears to be along-shore uniform, but a smaller area along-shore distance was surveyed. Google Earth imagery collected in 2010 through 2018 shows that sand bars vary from complex three-dimension structures (Figure 12a-2010 & b-2016) to highly along-shore uniform (Figure 12c-2017). Imagery collected on 10/5/2018 appears to show more topographic variability in the region with 50 m of the beach than the 10/26/2018 UAV survey, indicating that the three wave events with Hs > 2 m during the three-week period between the two data sets may have changed the near shore topography. Results from the subsequent surveys in the 2018 deployment will be discussed in section 4.1.2.

A.

B.

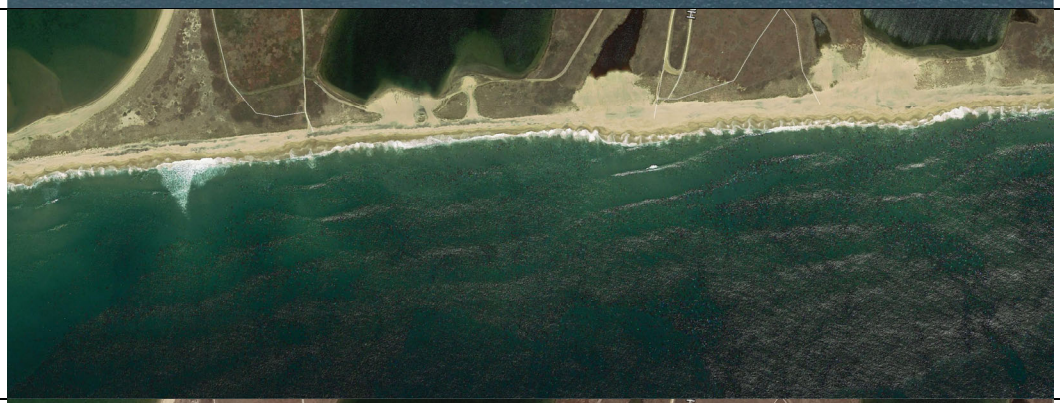

C.

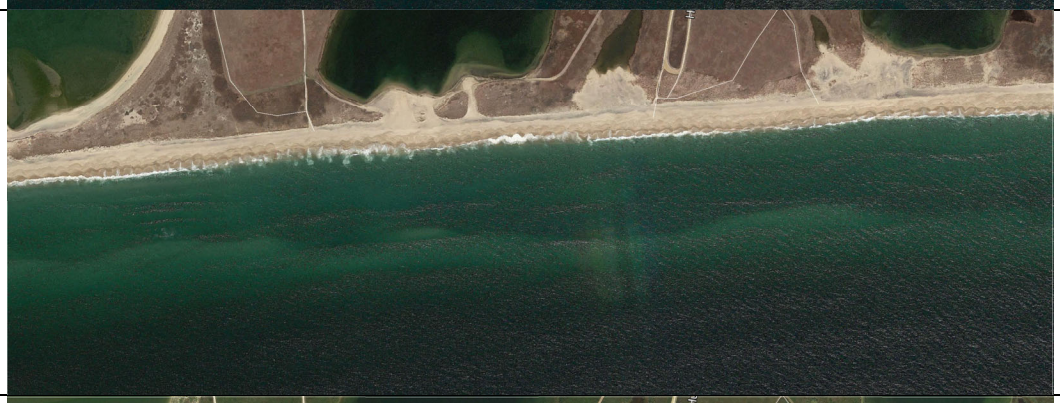

D.

Figure 12. Google Earth Imagery of Long Point A) 12/30/2010, B) 5/10/2016 C) 4/14/2017 D) 10/05/2018. Red boxes indicate areas surveyed in 2014 and 2018 shown in Figure 11.

3.3.3. Combined Doppler and USBL Based sUXO Tracking

As shown in Figure 10, an acoustic ultra-short base line (USBL) array was mounted in the hull of the ASV. The array was based on a general purpose high frequency acoustic development board built at WHOI ([14]). Each channel was sampled at 24Mhz, demodulated to 40 kHz, based on the center frequencies of the active pingers on the sUXO, and decimated by a factor of 480, resulting at an output sample frequency of F_s =50 kHz, thus each τ = 50 mS long ping from the transmitters are sampled with $N = \tau F_s$. The signals are demodulated to baseband and decimated, with filtering a 20 kHz bandwidth so all the signals in the 30 to 40 kHz pinger frequency range are retained for post processing. The array is operated in a receive only mode and recorded data continuously while the boat was in the water and ping detection was conducted in post-processing. The USBL data logger was time synced with the echosounder/GPS PC datalogger at the beginning of each survey, and transmitted time stamps to the PC datalogger once per second to ensure time synchronicity was maintained. The IMU is the Pixhawk autopilot also recorded data with GPS time stamps so that position, attitude and USBL receptions could all be analyzed with a common time base.

The USBL had 4 elements based on the maximum number of channels on the data recorder which were non-uniformly spaced to maximize the aperture with best side-lobe performance according to minimum redundancy linear array (MRLA) design principles [15]. The elements were located a x_s = [-3.0 -2.0 0.9 3.0] * s_p with x = 0 the center of the array and a spacing of sp =.016 which is slightly smaller than $\lambda/2$ = 0.019 at 40 kHz, due to constraints on the physical dimensions of the previously designed circuit board, which allowed a 9.6 cm long array . An equivalent uniformly sampled array with Nyquist element spacing would have element locations at x_s = [1.5 -0.5 0.5 1.5] * s_p for a total array length of 4.8 cm.

In post-processing, the 50 kHz sampled data that had been demodulated to 40 kHz during collection was demodulated by a series of frequencies in the range from 0 to 10 kHz separated by 1 kHz to search from transmissions from individual pingers and filtered with a 200 Hz band with filter to reject signals from the other pingers. Initial detection of received pings was performed by filtering the sum of the amplitude from the 4 channels with a 60 s duration boxcar train filter with 50 ms pulses 1 s apart based on the transmitted signal from the pingers. Peaks in the output of this filtering operation were used as starting locations to extract 50 ms of data from each channel. Typically, on the order of 2000 peaks were found in a one-hour survey in the vicinity of the pingers, although some peaks were associated with low SNR receptions due to the long (60s) ping detection filter.

Each 50 ms snippet of data ($x_i[n]$) is first examined for Doppler shift since the ASV is traveling at speeds of approximately $|\overrightarrow{v_b}|$= 0.5 to 2 m/s, frequency shifts of up to $f_d = |\overrightarrow{v_b}|f_c/C = 60\ Hz$ are possible. The doppler compensated signal is

$$B_{Doppler}\left(f_c \frac{|\overrightarrow{v_b}|cos\theta_{rel}}{C}\right) = B_{Doppler}(f_d) = \sum_{i=0}^{3}\left|\sum_{n=0}^{N-1} x_i[n]e^{-jnf_d/F_s}\right| \qquad (11)$$

where f_d is varied from – 60 to 60 in 1 Hz steps. The spectral response of the Doppler processing to both data and to a simulated input signal is shown in figure 13c&d. The response to simulated signal is:

$$B_{Doppler}(f_d) = \frac{sin(\pi f_d \tau)}{sin(\pi f_d \tau/N)} = \frac{sin(\pi f_s\, cos(\theta_{rel})|\overrightarrow{v_r}|\tau/c)}{sin(\pi f_s\, cos(\theta_{rel})|\overrightarrow{v_r}|\tau/Nc)} \quad (12)$$

The magnitude of the Doppler compensated signal summed over all four channels $B_{Doppler}(f_d)$ can be used to examine the frequency shift of the signal before subsequent beamforming operations. The Doppler shift from positive to negative is clearly seen as the ASV passes the target at t = 770 s (Figure 13).

Beamforming is conducted by calculating the inner product of a steering vector (s_v) with the doppler compensated signal (d_d) at the peak of the Doppler spectra for each ping reception:

$$B_{USBL}(\theta_s) = \sum_{i=0}^{i=3} X_i[f_r] e^{-j2\pi f_r x_s[i] cos\theta_s/c} \quad (13)$$

where θ is varied from -90 to 90 degrees since the beam pattern is symmetric on either side of the line array. The shift in beam angle from negative to positive, passing through broadside (0°) is clearly seen as the ASV passes the target at t = 770 s (Figure 14).

A solution based on simulated input data to Eqn (13 can be found by using the Fourier transform of a uniform pulse of length τ for $X_i[f_r]$. (Figure 14). The Doppler spectra has much better side lobe performance than the USBL response due to the choice of MRLA array for the USBL which maximizes aperture (minimizes beam width) at the expense of higher side lobe levels. At a

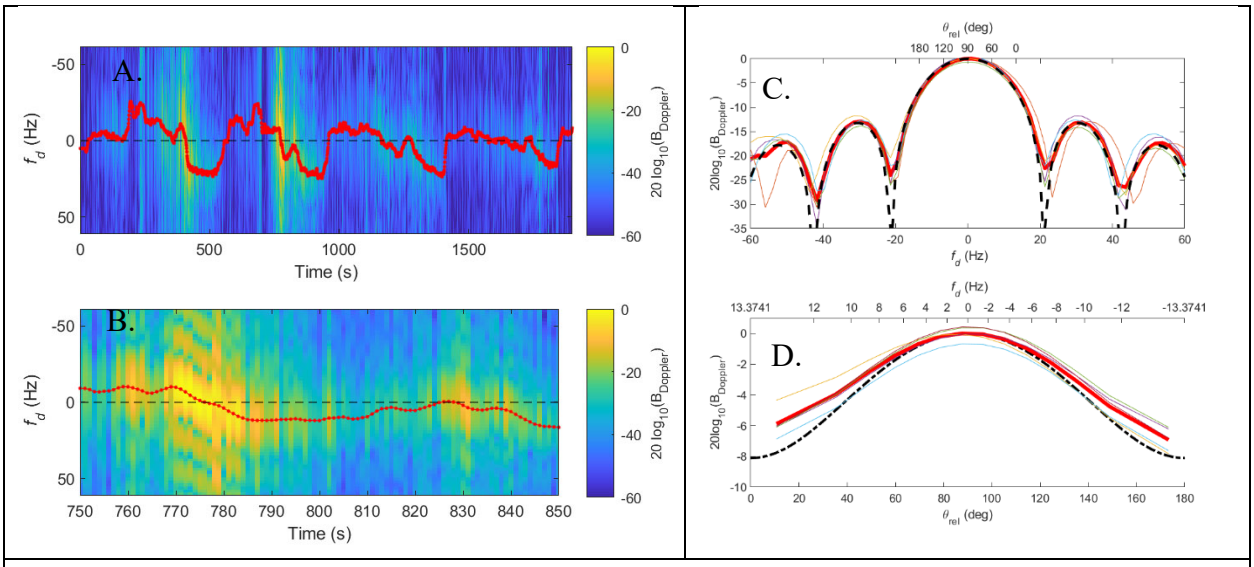

Figure 13. Doppler shift of the pings received on the USBL array. The color represents the magnitude of y_d, and the red line is a time series of the peak of the Doppler spectra. A) Entire Survey, B) From 750 to 850 seconds as the ASV passes the target emitting at 34 kHz. c) Doppler Shift Spectra for 5 pings near the target (t=771 to 775 s) and average of the 5 pings (thick red line) plotted vs Doppler Shift Frequency (f_d) The angular coordinates transformed from Doppler Shift Via Eqn 25 is shown above the plot on the upper x-axis. Predicted Spectra from frequency domain theory is shown as a black dotted line. All spectra are shifted to have peaks at f_d = 0. Lower Panel: Doppler Shift Beam patterns for 5 pings near the target (t=771 to 775 s) and average of the 5 pings (thick red line) spatial domain theory is shown as a black dotted line}

receiver speed of $|\overrightarrow{v_b}|=$ 2 m/s the synthetic aperture of the Doppler with the 50 ms pings would be 0.10 m, so almost the same as physical length of the array (0.09 m); however, in this survey the ASV was travelling 0.6 m/s as it passed the target resulting in a synthetic (Doppler) aperture of 1/3 of the physical aperture of the array.

The Doppler measurements can be transformed into a bearing relative to the vessel by using the ASV's velocity and heading. The Doppler velocity is calculated by

$$f_d = f_s \frac{|\overrightarrow{v_r}| cos\theta_{rel}}{c} \tag{14}$$

The projection of the Doppler velocity onto the true velocity measured accurately by the PPK GPS gives the bearing relative to the vessel $\theta_{rel} = \cos^{-1}(V_d/V_{GPS})$. This can be transformed into a geographic Cartesian bearing by $\theta_{dG} = \theta_{rel} + \theta_{GPS}$ where $\theta_{GPS} = \tan^{-1}(u_{GPS}/v_{GPS})$ and u_{GPS}, v_{GPS} are the easterly and northerly components of the GPS measured vessel velocity. This measurement of velocity heading is independent of the vessel heading and is a higher quality measurement than the vessel heading due to the accuracy of the PPK GPS method for velocity heading vs the accuracy of the low cost IMU in the pixhawk for vessel heading. The Doppler spectra as a function of frequency can also be transformed to a function of bearing via a similar transformation.

The USBL bearing spectra $D_b(\theta_{usbl})$ can be transformed to a similar cartesian geographic spectra by substituting $\theta_{usblG} = \theta_{usblG} + \theta_{IMU}$, where θ_{IMU} is the direction from the IMU, which is based on an Extended Kalman Filter (EKF) fusion of magnetometer, accelerometer, gyroscope and code resolving GPS data.

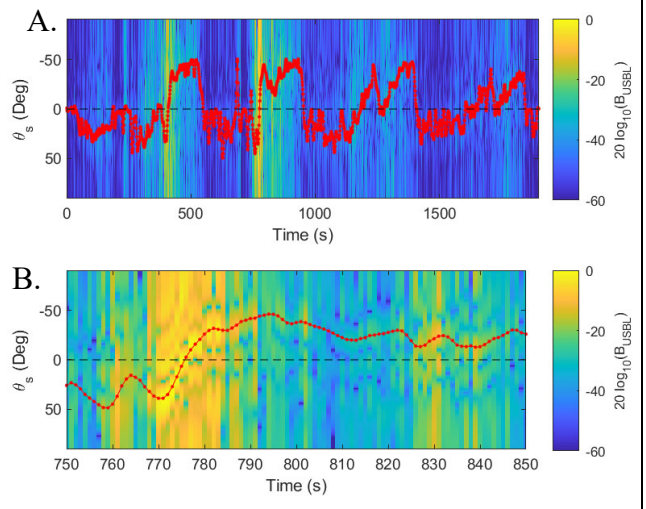

Figure 14. Beamforming of the pings received on the USBL array after Doppler compensation. The color represents the magnitude of y_b, and the red line is a time series of the peak of the beamformer angular spectra. A) Entire Survey, B) From 650 to 850 seconds as the ASV passes the target emitting at 34 kHz. C) USBL Beam Pattern for 5 pings near the target (t=771 to 775 s) and average of the 5 pings (thick red line). Predicted Beam Pattern from theory is shown as a black dotted line. All Beam Patterns are shifted to have peaks at q_s = 90.

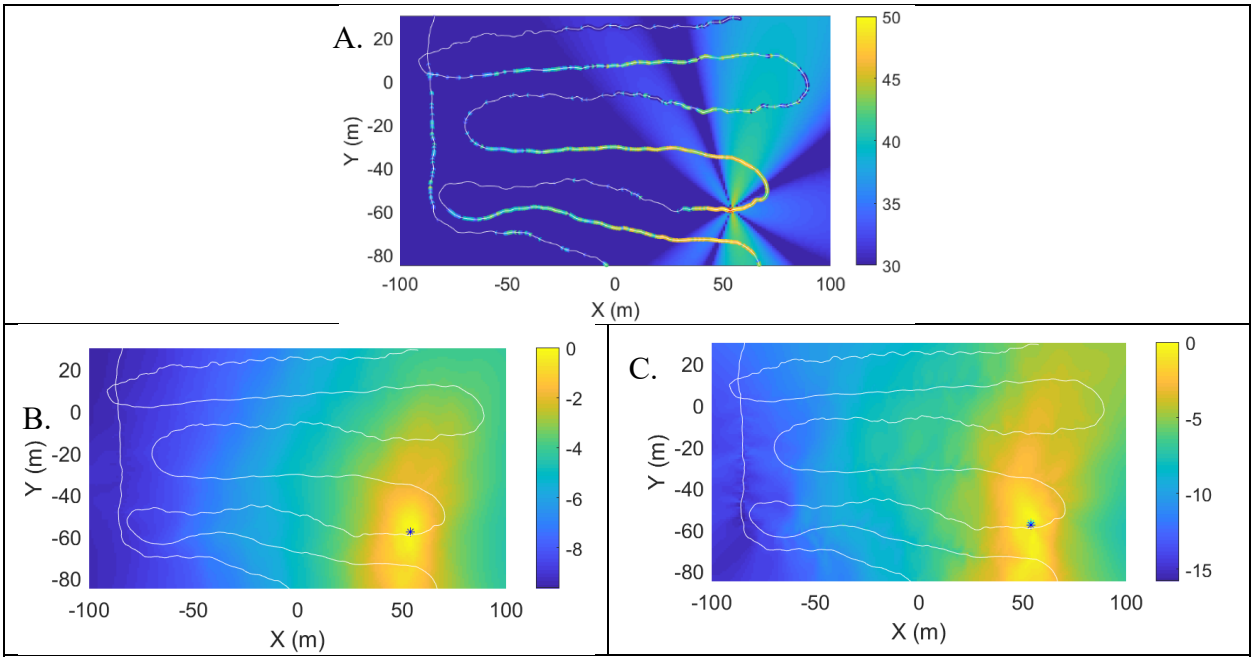

Figure 15 A) Gridded Doppler beam pattern for an individual ping near one of the Targets. B) Sum of all gridded Doppler beam pattern with a blue marker at the location of the target estimated by the peak of the sum. C) Sum of all gridded USBL beam pattern with a blue marker at the location of the target estimated by the peak of the sum from the Doppler estimates and a cyan marker for the USBL estimates.

These directional spectral estimates can be centered on the vessel's position for each ping reception and then multiple receptions with different positions can be combined to estimate the target location via triangulation. For an individual reception the direction spectra is transformed to a spatial pattern on a fixed *x,y* grid via $G_D(x,y) = \frac{D_d(\theta_G)}{R+3}$, where $R = \sqrt{(x-x_{GPS})^2 + (y-y_{GPS})^2}$ and $\theta_G = \tan^{-1}((x-x_{GPS})/(y-y_{GPS}))$. The addition of 3 prevents singularities at the vessel's location and compensates for near field beam processes. The gridded Doppler direction spectra along with the path of the ASV for a single reception near the location where the vessel is broadside to a target is shown in Figure 15a.

To estimate the position of the target the gridded beam pattern from all ping receptions is summed. The peak of this sum is the position estimate. This bearing only estimate of position effectively triangulates the location of the target from multiple bearing estimates. (Figure 15b). Similar calculations can be performed for the USBL based gridded beam patterns. The sum of the USBL based gridded beam patterns for one target is shown in Figure 15c. The blue marker represents the peak from the Doppler based calculations and the Cyan marker is from the USBL based calculations. For this target the two estimated locations are 1 m apart. A combined solution is obtained by summing the Doppler based beam gridded patterns and the USBL based gridded beam patterns and estimating the position of the targets from the peak sum of the gridded solutions. These positions were compared to GPS locations of small buoys attached to the target, which may vary from the actual position by up to 5 m due to buoy line scope (Figure 16).

The r.m.s. error between the combined USBL and Doppler estimates with the GPS Buoy measurements is 3.9 m and the 85th percentile is 5 m. Based on these error magnitudes this technique is suitable for measuring large scale migration of the sUXO on scales of sand bar and surf zone with (~100 m), but cannot measure small position and orientation changes on the scale of the objects themselves (~1 m) as the object roll or shift near the threshold of motion.

3.4. **Measurement Techniques for Forcing Hydrodynamics**

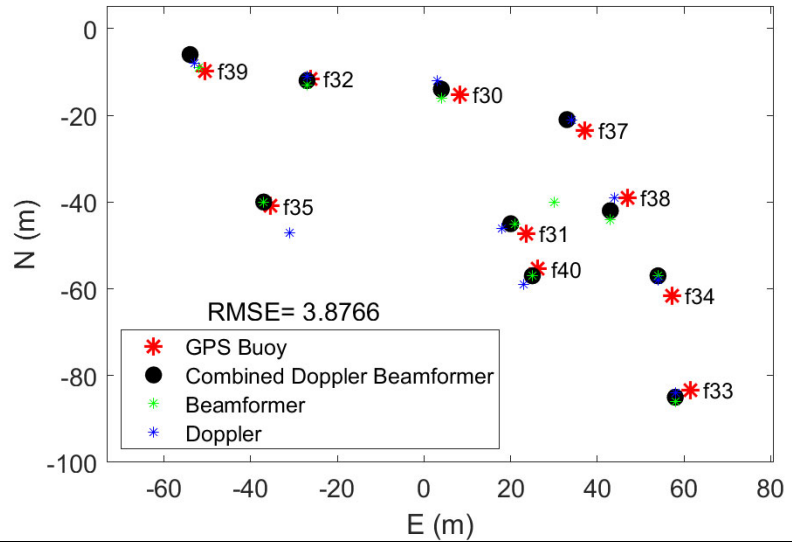

Figure 16. Results of gridded tracking from GPS Buoys (Red stars), Combined Doppler and Beamforming (Black Dots), Beamforming Only (Green Stars), Doppler Only (Blue Stars). The targets are labelled by pinger frequency in kHz.

Due to the failure of the 2 m high quadpod during the 2014 long point deployment and the difficulty in bringing large enough ships to deploy such a frame into the outer regions of the surf-zone, in 2018 only pole mounted sensors were used. The 2.5 m long poles were jetted 2 m into the sand bed at a 2 m and 4 m depth location (Figure 11). Nortek Vector Velocimeters with pressure gauges were mounted on the poles with the sampling volume approximately 75 cm above the seafloor. The Vectors were set to sample at 8 Hz for 10 minutes starting every 30 minutes to save battery power. In addition to the Vectors, four Lowell Engineering Tilting Current Meters with Pressure (TCMP) sensors were deployed in the region where sUXO placement was planned. The TCMP were deployed on small (50 cm wide) weighted frames which could bury or settle during erosion. A 30 cm pole was attached to the frame so slight burial would not restrict the motion of the tilting sensor. Calibration tests of these instruments and comparison to the nearby Vector show that these sensors can measure velocities associated with low frequency waves (T > 8s), but that high higher frequencies are damped with a linear decrease with respect to frequency. Averaging the wave motions produced similar estimates of mean currents to the nearby Vectors.

A small Spotter wave buoy ([16]) was also deployed in 13 m water depth, 1.6 km offshore of the study site, to measure offshore wave conditions and telemeter the data back to shore via an Iridium satellite link. This data can be used for initialization of offshore boundary conditions for wave models and in real-time for planning response to large wave events. The buoy was deployed with a double catenary mooring design as described on the Spotter web pages. The

weights on the catenary were increased by 30% to account for the anticipated higher wind conditions at the Martha's Vineyard site.

4. Results and Discussion

4.1. **Hydrodynamic Forcing**

4.1.1. Offshore Wave Measurements

Measurements of wave height from the Spotter buoy indicated that the waves were small (*Hm0* = 0.5 to 1 m) from when it was installed on Oct 23st until the sUXO deployment and Bathymetric Survey 1 on Oct 26th (Figure 17). On Oct 27th the waves rapidly increased to *Hm0* = 3.8 m, T_p =12.8 s with peak direction veering from SW (244°) to ESE (110°) and the back to S (180°) as the storm passed. Once the waves decreased enough to make ASV operations feasible, a second survey was conducted. A series of wave events with *Hm0* = 2 to 3 m occurred before the third survey on Nov 15th. Wave height, Hm0 scale by 0.6 to match the Spotter data from the CDIP buoy off Block Island is also shown for data before the Spotter deployment. The CDIP buoy is located further offshore in 50 m water, thus the factor of 0.6 is an empirical attenuation factor.

Wave measurements from within the surf zone (Figure 18) show wave heights that correlate with tidal water depth as more wave energy is dissipated due to wave breaking offshore of the measurement site at low tide. During the energetic storm on Oct 28th wave height reached 2 m at this site, which is substantially attenuated from the 3.8 m wave height measurement at the 13 m isobath measured by the Spotter Buoy. The representative near bed orbital velocity reached a peak of 1 m/s at this site, and both velocity skewness and acceleration skewness were directed onshore with moderate levels of 0.0 to 0.04. Unfortunately, the ADV at the 4m site was set up

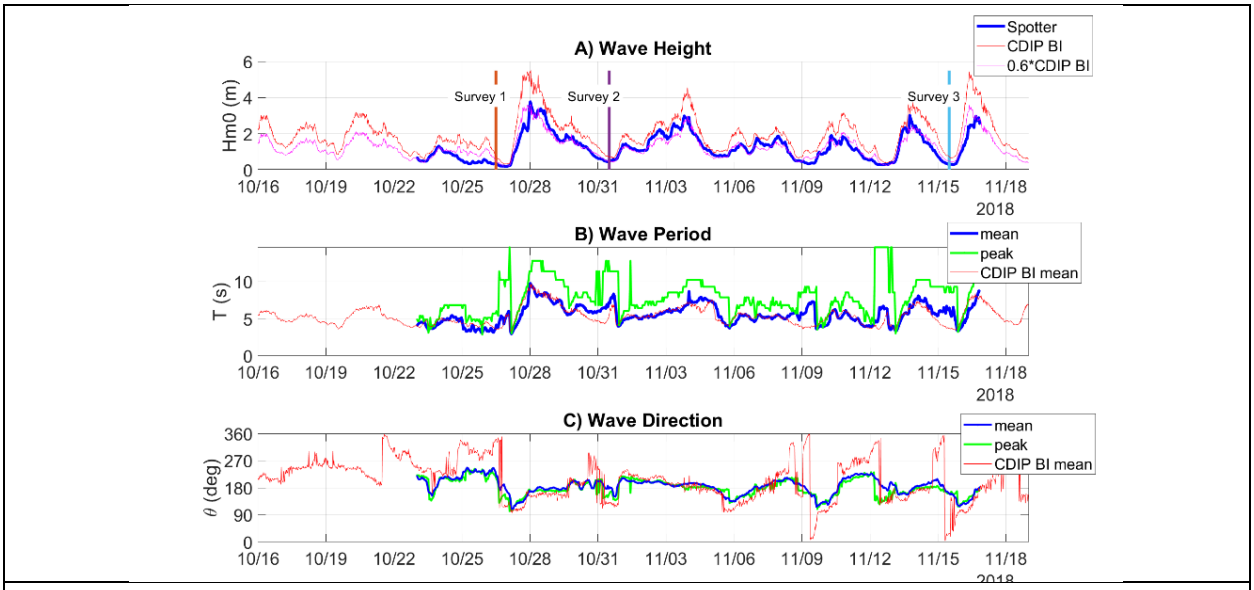

Figure 17. A) Wave Height (Hm0) from the Spotter Buoy, CDIP Buoy and CDIP data scaled by 0.6. B) Mean (blue line) and Peak (green line) Wave Period from the Spotter buoy and CDIP buoy (red line). C) Wave direction with the same line types as B.

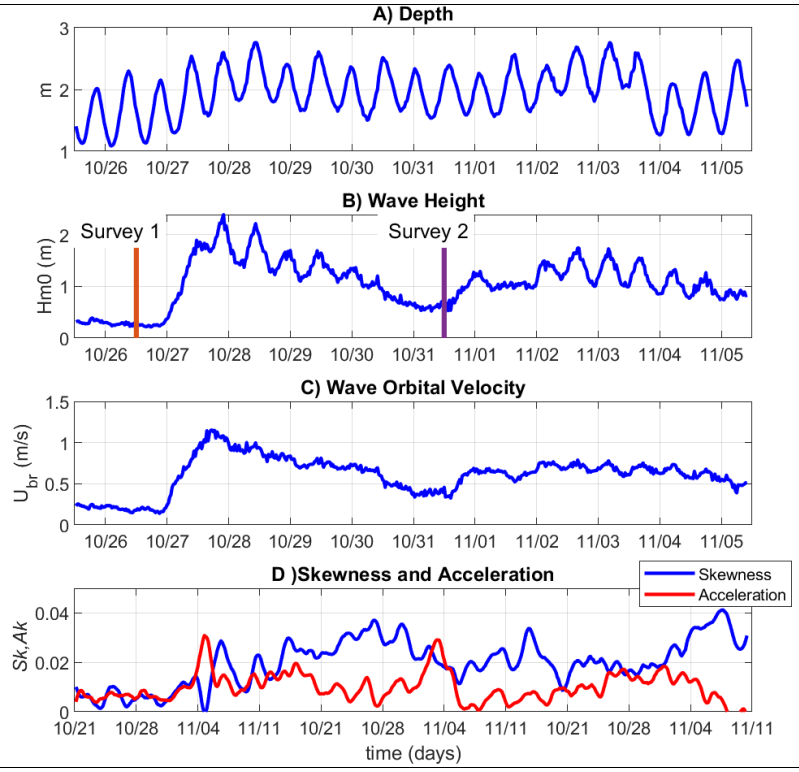

Figure 18. Wave measurements inside the surf zone from the Vector ADV located in 2 m water depth. A) Depth, B) Wave Height, C) Wave Orbital Velocity, and D) Skewness and Acceleration.

incorrectly and did not start until after the Oct27th wave event in which it was partially buried by a migrating sand bar.

Measurements of mean currents in the surf zone from the ADV and the TCMPs are compared in Figure 19. The eastward (along-shore) and northward (across-shore) from the ADV in 2 m water depth and the nearby TCMP1 produce similar measurements of mean current. This is encouraging because it was not known a-priori if the TCMPs could successfully average the waves due to the non-linear response to the sensor to high frequency oscillatory flows. The along shore flows are initially directed to the West with speeds of up to 1.5 m/s and then transition to the East with weaker speeds of 0.5 m/s as expected with waves initially from the East and then transitioning to a direction from the South (Figure 19a). During the peak of the storm there are strong offshore mean flows with speeds of up 0.7 m/s at the 4 m TCMP site and 0.4 m/s 2 m TCMP site (Figure 19b). These are most likely return flows due to the strong onshore stokes drift associated with the large waves. Wave measurements from the pressure sensors are similar for all the instruments, although mean water depth from TCMP does become deeper throughout the deployment since the TCMPs were mounted on weighted platforms that rested on the seabed, and would follow the sand surface during erosion. The ADVs were mounted on poles jetted into the seafloor which do not move vertically.

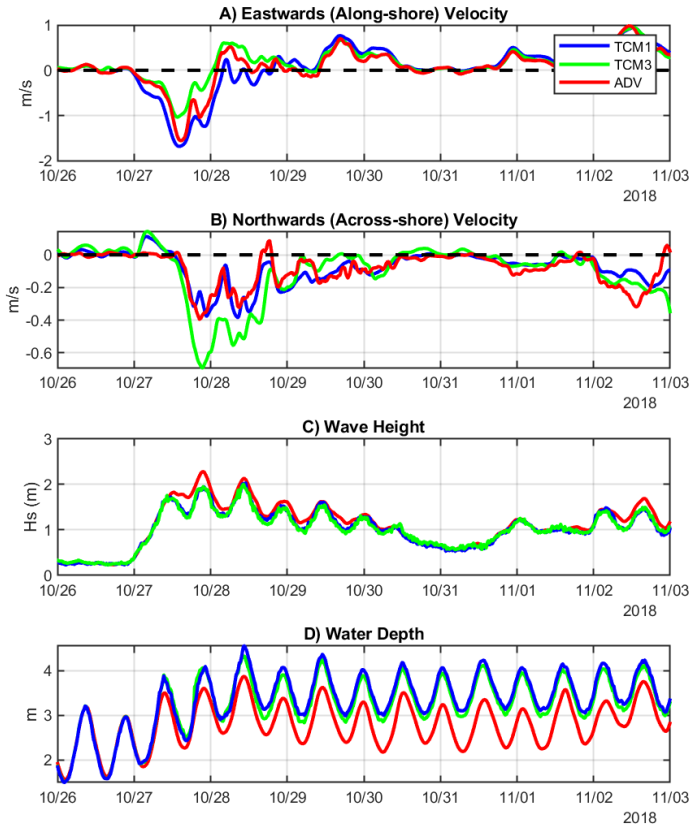

Figure 19. Measurements from the TCMPs with ADV data for reference. A) Eastward mean flows, B) Northward Mean Flows, C) Wave Height from pressure, and D) Water Depth from pressure.

4.1.2. Sand Bar Migration

Three repeat topo-bathymetric surveys taken with the surf zone ASV combined with the walking GPS beach surveys before the 10/28 wave event (survey 1, 10/26), after the 10/28 wave event (Survey 2, 10/31) and two weeks after the event (Survey 3, 11/15) reveal dramatic changes in sand bar morphology in response to the large waves and offshore return flows (Figure 20). Before the 10/28 wave event the sand bar is located at Y=100 to 110 m and the crest is 1.4 to 1.5 m below z=0. This location is most likely in equilibrium with a series of 2 m wave height events that occurred in the two weeks prior to the survey (Figure 17). During the 10/26 survey, the sand bar migrated 50 m offshore to Y= 60 m, in response to the further offshore break point of the 3.8 m high waves during this event and strong offshore directed return flows. The depth of the crest is - 2.4 to 2.5 m. In the two weeks between surveys 2 and 3, which featured four 2 to 3 m high wave events, the sand bar did not migrate further offshore, but did become slightly less along-shore uniform, and the trough onshore of the bar deepened slightly. Elevation Difference (ΔZ) maps and transects for the 10/31 – 10/26 surveys, indicate 1 m of erosion at Y=110 to 120 m and up to 1.5 m of deposition at Y =50 m (Figure 21).

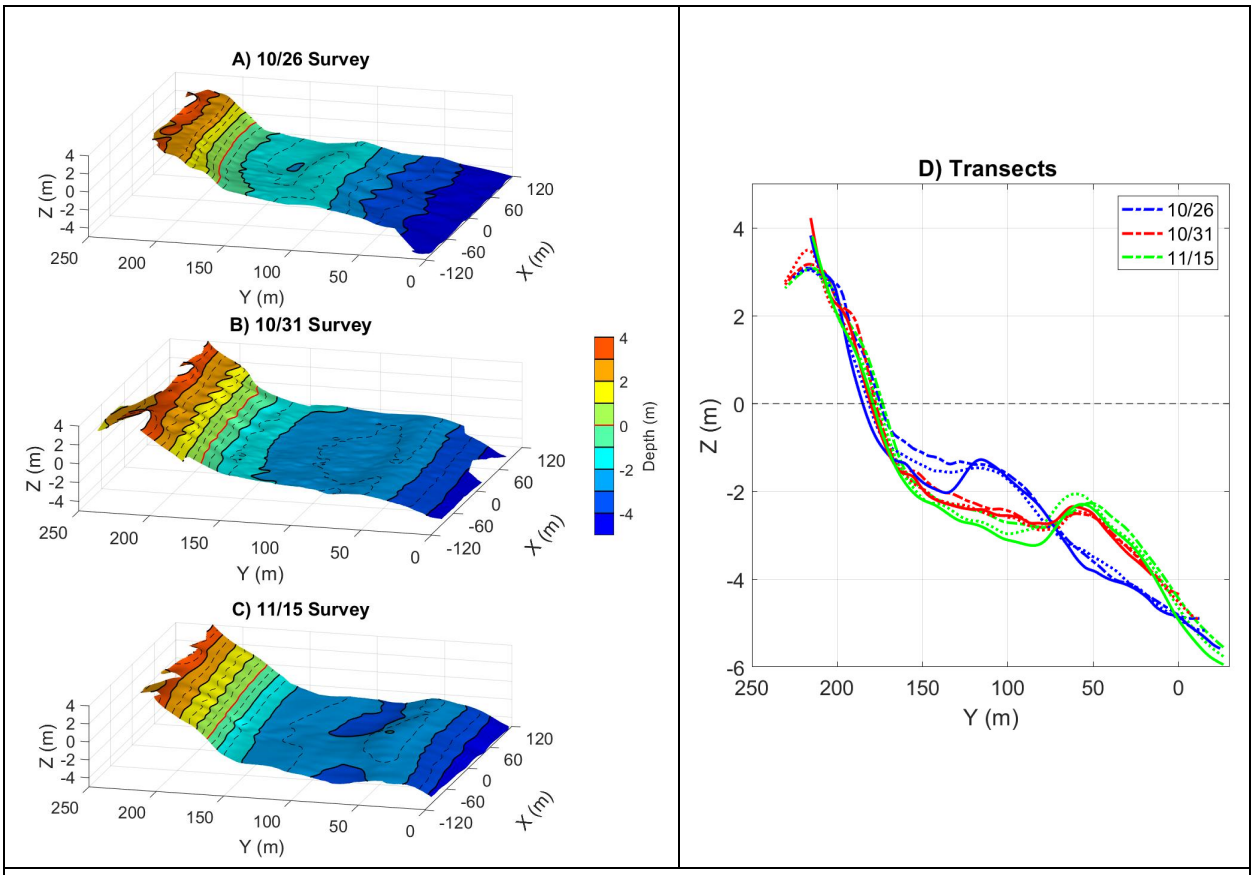

Figure 20. Topo-Bathymetry measurements with elevation relative to NAVD88. A-C) Topo-Bathymetric surfaces from the three surveys with 1 m spaced contours (solid lines), 0.5 m contours (dashed lines), and the red line indicates the z=0 contour level. D) Cross-Shore Transects from X= -40 mS(solid) ,0 m (dotted) and 40 m (dashed) for the three surveys.

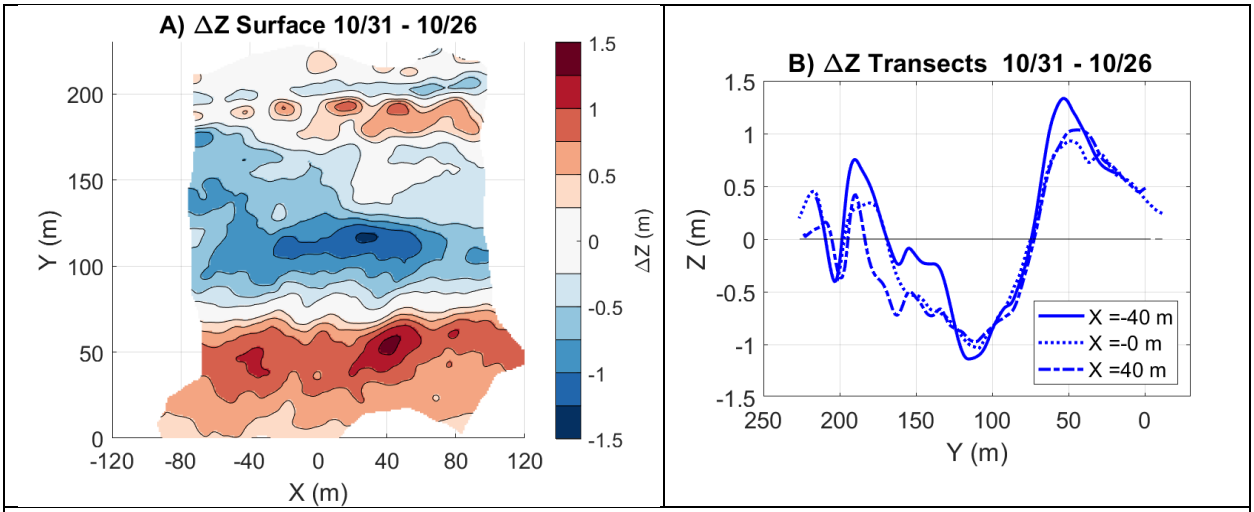

Figure 21. Topo-Bathymetry elevation difference (ΔZ) measurements for the 10/31 – 10/26 surveys. A) Difference map with red indicated deposition, and red erosion. B) Transects of ΔZ at X= -40 mS(solid) ,0 m (dotted) and 40 m (dashed)

4.1.3. sUXO Surrogate Deployments, Large Scale Mobility and Burial

Sixteen sUXO were deployed in water depths ranging 3 to 4.5 m, offshore of the sandbar on 10/26 (Figure 22). The labels for the various objects (e.g. LLA: Large Diameter, Light Density, Series A) is described in Section 3.2. Green stars indicate the deployment location and Yellow stars are the final locations for objects that migrated. If the final location was within 4 m of the deployment location a yellow star was not plotted. These small location differences were within the measurement error of both the tethered buoy GPS fixes, due to tether scope, and the USBL/Doppler tracking methods. Most of the sUXO (8 out of 16) migrated less than 4 m. Four sUXO (LVLB, LLB, LMA, SMA, LHB, SMB, LHB, and SHB) migrated between 4 and 10 m, typically in the NNW direction in response to waves from the SSE at the peak of the 10/28 storm. One sUXO (LMB) migrated 21 m to the NNW. The migration distance does not appear to be related to density as all density classes contained sUXO that both did and did not migrate. The range of density classes was relatively narrow with "Very Light" (VL) set at density relative to seawater of $S = 2.25$ and "Heavy" (H) set at $S = 3.0$. Based on the results of MR-2320 this is the transitional regime where some object migrated, and others did not on the previous measurements. (Figure 2). The relatively low migration rates are most likely a consequence of the strong offshore flows and will be discussed further in section 4.2.

Burial was dominated by the offshore sand bar migration and both instrument (TCM2, ADV4 and TCM4) and sUXO depths below the sand surface at recovery were consistent with sand deposition as shown in the difference map (Figure 22). Any additional burial due to scour or

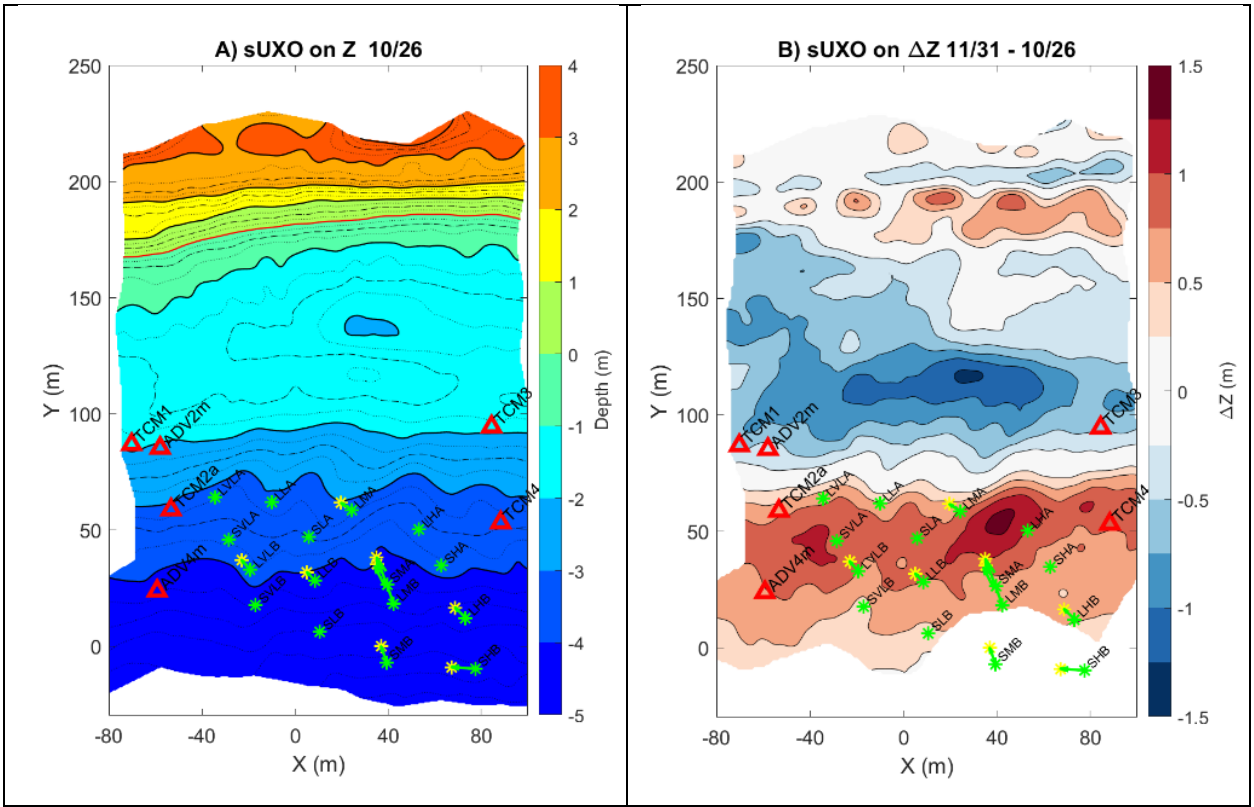

Figure 22. sUXO and instrument deployment (Green *) and final locations if migration occurred (Yellow *) on A) Topo-Bathymetry maps and B) elevation difference (ΔZ) maps

other burial processes was not within the accuracy of the diver-based burial measurements during recovery.

4.1.3.1. Surrogate Small-Scale Mobility

The embed accelerometers, pressure sensors and ambient light sensors in 5 of the sUXO provide information on small scale mobility and time of initial burial relative to wave and tidal forcing (Figure 23).The light sensors, which record ambient light, show 100% values during daylight hours of Oct. 26 and then readings of a few percent on Oct 28th at the beginning of the energetic wave event. The LMB sensor shows light level variability for 5 hours after the others reach their minimum values, consistent with longer duration in roll variability and the increased migration of this object relative to the others. All of the sUXO show a decrease in pressure relative to the pole mounted ADV pressure sensor and small-scale roll variations at the beginning of the storm (before the solid black line). The relative pressure was set to zero at the beginning of the deployment by subtracting the mean of the first day and the ADV was located in 2 m water depth, 50 m onshore of the sUXO. This indicates these sUXO were mobile (e.g. rolling back and forth due to wave forcing, consistent with time dependent mobility model predictions, Section 2.1.1), although some did not migrate distances greater than 5 m based on GPS tracking. The relative pressure measurements also indicate there was most likely some erosion and that the sUXO became deeper on the erosive surface before the large amount of deposition associated with offshore migrating sandbars. The increase in depth is not due to burial at this initial stage of the wave event due the optical measurements and roll variability indicating mobility. As roll

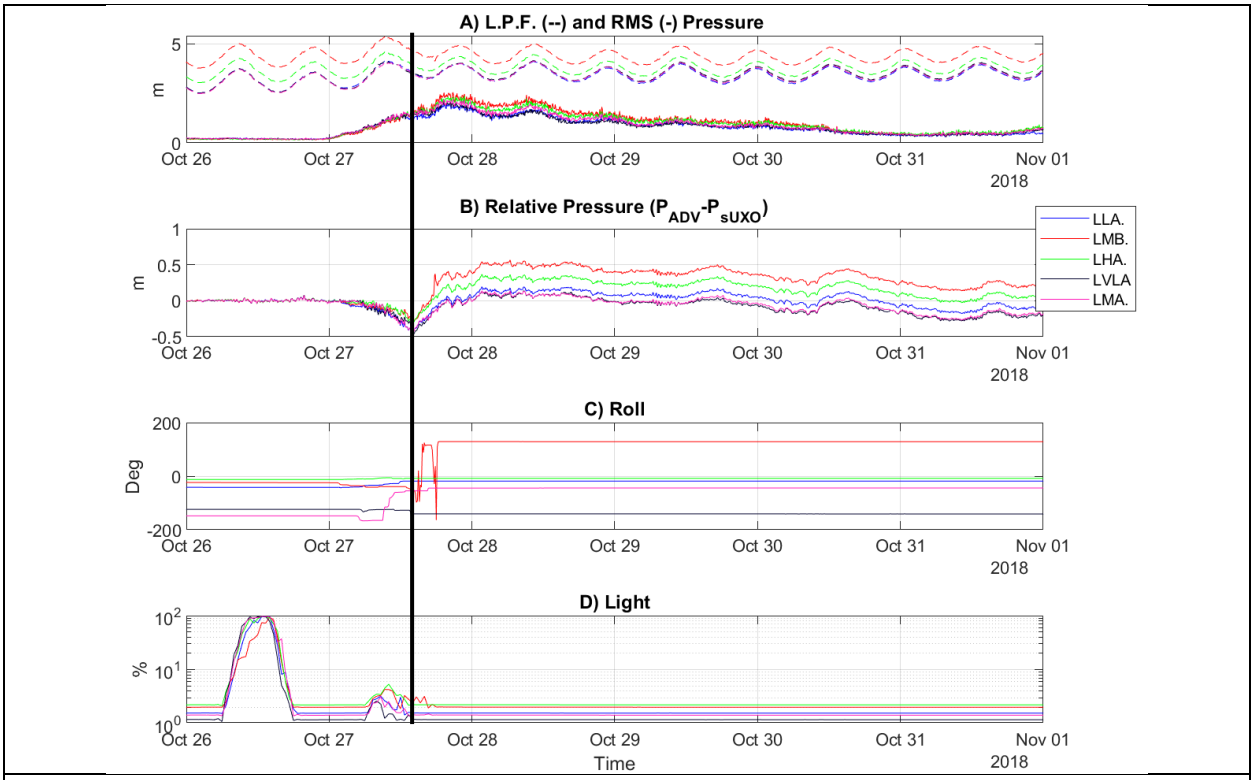

Figure 23. A) Tide resovling Low Pass Filtered (L.P.F-dashed lines) and sliding window RMS pressure from each sUXO. B) Pressure relative to a reference from the ADV sesnor on a fixed pole mount, + indicates the sUXO is becoming shallower than the reference. C) Roll and D) Light from the sUXO embedded sensors. At solid black line indicates Oct 27, 14:00 hours at the minimum of relative pressure.

variations stop and light falls to zero, indicating the sUXO are becoming buried by the migrating sandbar, the relative pressure increases by different amounts for each object. This may indicate there is some upward motion of the sUXO in the initial stages of deposition associated with the migrating sand bar.

4.2. **Numerical Modeling of sUXO Migration**

In order to understand the relatively small sUXO migration in the 2018 measurements with large waves compared to the large onshore migration observed in 2014 with medium waves, the equations describing object migration and burial (Section 2.1) were forced with wave resolving near bed velocity output from the SWASH numerical surf-zone hydrodynamics models. SWASH (Simulating WAves till Shore, [17]) is a non-hydrostatic, free surface, depth-resolving model that is ideally suited for modeling wave transformation across the surf-zone and return currents that may force UXO migration. The model run is 2D mode with 10 vertical layers, and 1200 across shore cells with 1 m resolution. The model was forced with a modified Jonswap spectra consistent with conditions at the peak of the largest 2014 (*Hs* =2.5 m, *Tp* = 11 s) and 2018 (*Hs* =4.0 m, *Tp* = 12 s) wave events at the offshore boundary located in 12.5 m water depth, and for a variety of other wave heights. The bottom boundary input was calculated by averaging 50 m of alongshore data from the 2014 bathymetry surveys.

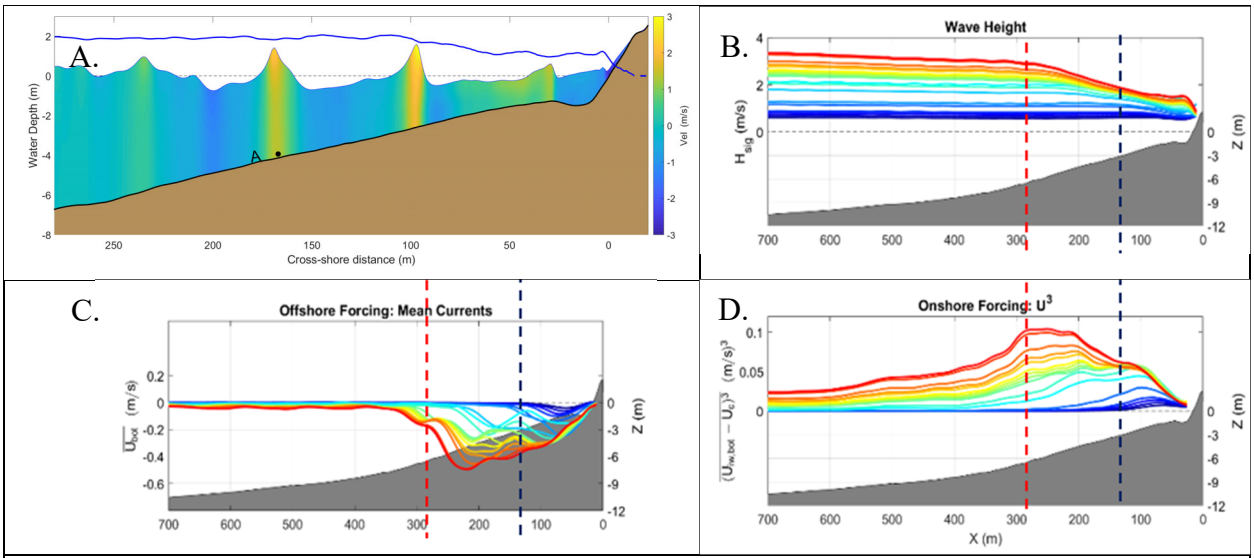

Figure 24. A) Temporal snapshot of cross-shore velocity output from the SWASH model. B-D) SWASH model results for a range of input wave heights color coded from blue with *Hs* = 1 m to red with *Hs*=3.5 m. The blue and red dashed line represents the offshore extent of the surf

zone and the approximate balance point between onshore and offshore directed forcing for small waves and large wave respectively.

A temporal snapshot of the model output is shown in Figure 24A for a case with input of *Hs* =2.0 m, with a seed UXO located at x= 160 m. The waves offshore of 150 m have high velocity skewness (short periods of high velocity under the crest and longer periods of low velocity under the trough), but relatively weak onshore-onshore asymmetry. In contrast, the wave at x = 100 m has high asymmetry with a steep front and high skewness with velocities under the crest of ~ 2 m/s. While the wave at x = 40 m still has high asymmetry, it has broken, dissipated energy and reduced height. Simulations run over a range of wave heights from *Hs* = 1 to 3.5 m, show the break point as defined by the location where the wave height begins to decrease moves offshore from x = 120 m (blue dashed vertical line) to x = 260 m (red dashed vertical line) as wave height is increased (Figure 24B). The offshore directed return currents reach a peak speed just onshore of the break point and begin to decrease further offshore. The magnitude of offshore flow of 0.4 to 0.5 m/s under the most energetic conditions simulated is roughly consistent with measured offshore flows of 0.5 to 0.6 m/s (Figure 19). This location also moves offshore as wave height increases (Figure 24C). The peak in wave skewness also occurs near the breakpoint (Figure 24D). The values of skewness at 2 m depth predicted by the model (S_k ~ 0.050) are slightly larger than observed values of S_k ~ 0.03. This discrepancy is most likely due to the model being run on 2014 input bathymetry which did not have an offshore bar which would cause waves to break and reduce skewness onshore of the break point. We anticipate that the final resting location of mobile UXO will be at a point where there is a balance between onshore forcing by wave skewness, acceleration and offshore return flows so that with large waves the UXO would be trapped near the red vertical line and for smaller waves near the blue vertical line.

The hydrodynamic output of wave resolved near bed velocities from the SWASH model forced with conditions consistent with conditions at the peak of the largest 2014 (*Hs* =2.5 m) and 2018 (*Hs* =4.0 m) surveys was used as input to the UXO migration model described by equations in

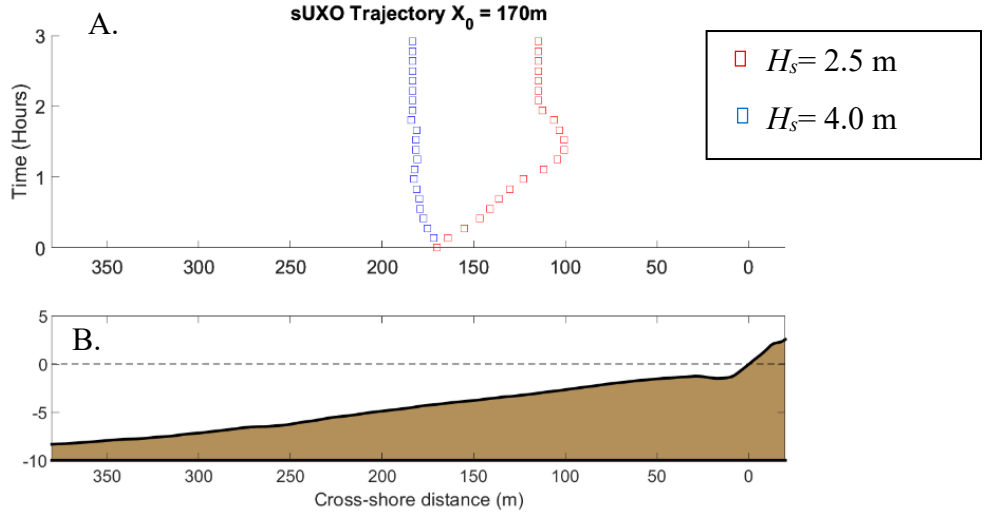

Figure 25. Results of the UXO migration model forced by SWASH hydrodynamics output for 2014/2018 MV experiments with large input waves (*Hs*=4.0 m) representing 2018 and smaller waves representing (*Hs* = 2.5 m) 2014. A) sUXO trajectories, B) SWASH model input bathymetry

Section 2.1 . A UXO with relative density $S = 2.0$ was initially placed in the model domain at x= 170 m, depth = -4.0 m consistent with the deployment locations in the measurements. As expected from the changes in the break point for large and small waves and the associated change in the location of the offshore extent of the return currents in the case with large waves, the UXO migrated slightly offshore, and in the case with smaller waves the UXO migrated onshore 50 m. These results are consistent with general trends in the observations where little migration was observed for UXO deployed in 4 m water depth during the large wave of 2018 and significant onshore migration was observed in the smaller waves of the 2014 data. The model output has yet to be analyzed in detail to relative roles of wave skewness, acceleration and returns flows in determining the final resting locations, nor have a wide range of UXO densities, initial conditions, and the temporal dynamics of the wave events been considered. However, the initial success of this modelling approach is encouraging for further development and is the topic of proposed future research.

5. Conclusions and Implications for Future Research/Implementation

In our previous study in 2014 (MR-2319) modelling results consistent with measurements indicated that the transition from UXO burial to mobility is a highly time dependent process. In environments with moderate wave energy for long periods of time, UXO could scour and bury before wave energy exceeded the threshold for initiation of motion for the UXO. In contrast, in environments with intermittent low and high energy, UXO could remain proud on the seafloor during low energy periods, and then be more likely to mobilize on sudden transitions to wave energy levels above the threshold of motion. Equilibrium models for the initiation of motion did not produce results consistent with the measurements, but a time dependent model could. Based on this result, in 2018 a rapid response mode of deployment was employed whereby sUXO were placed on the seafloor immediately before a very energetic event started. It was expected that this method of deployment would lead to large migration distances for low to medium density ($1.5 < S_0 < 3$) sUXO.

In the 2014 measurements, maximum offshore wave heights reached 2.5 m and low to medium density sUXO migrated up to 100 m onshore from the deployment location in 3 to 4 m into 1 to 2 m water depths. In the 2018 measurements, despite that the waves were larger with maximum offshore heights of 4.0 m, sUXO deployed in similar initial locations to the 2014 measurements migrated a maximum of 20 m. Most of the sUXO deployed in 2018 migrated less than 5 m, although embedded accelerometer measurements indicated they were mobile, with small roll motions due to the energetic wave forcing. Bathymetry measurements from a surf zone capable autonomous surface vessel (ASV) indicated a sand bar migrated offshore during the energetic wave event and deposited 1 to 1.5 m of sand at the sUXO deployment location, which deeply buried the sUXO.

To examine the physical mechanisms for the low migration distances in 2018, the parametrized initiation of motion models developed in MR-2319 was extended to model sUXO migration. The migration model was forced with waves and current output from the SWASH surf zone hydrodynamics numerical model. Both the measurements and the model show strong (~0.5 m/s) offshore directed “undertow” flows shoreward of the wave breaking location. The models show peaks of skewness near the break point. The parameterized migration model indicates sUXO migrate to a location where onshore directed forcing from skewness balances the offshore

directed forcing from undertow flows. This location is typically at the location where waves first begin to break (break point). In the 2014 measurements, with H_s = 2.5 m waves the sUXO were deployed offshore of the break point and migrated onshore consistent with model predictions. In 2018, with larger waves of H_s = 4.0 m, the sUXO were deployed at the break point and little migration was measured or predicted by the model. Sand bars follow similar hydrodynamic convergence dynamics to these sUXO which have densities just slightly larger than water saturated sand ($S_{ws} \sim 2.0$). In the 2018 measurements, the sand bar migrated from an onshore location in equilibrium with the break point of smaller waves proceeding the study, to a location in equilibrium with the offshore break point associated with H_s = 4.0 m waves, and thus burying all the sUXO at the peak of the storm. This suggests that the most likely location to find low to medium density mobile UXO are in depositional regions as they follow similar convergence dynamics to the sand. As indicated by the 2014 measurements and modelling, higher density UXO will not be mobile under most forcing and are more likely to bury at their initial location. The good agreement of modelling results with observations also indicates the nearshore hydrodynamic models such as SWASH, which have been developed for the past decade and are still being refined, have potential to predict short term (one to two wave events) low to medium density UXO migration at other wave forced locations and serve as valuable input into simpler statistical models such as the Underwater Munitions Expert System model (UnMES, [18]). For longer predictions of sUXO behavior, the near-shore hydrodynamics models will need to be coupled to morphology models to predict sand bar and shoreline dynamics since the burial and re-exposure of UXO is tightly linked to these processes.

In addition to research on UXO migration and surf zone dynamics, this study resulted in several technological developments. A surf zone capable ASV was developed and used to both measure bathymetric change in a safe efficient manner and to track mobile sUXO with active acoustic sources. Bearing only tracking algorithms were developed using the USBL array data on the ASV and a novel Doppler based method. The Doppler based method can be used with a single transducer and has implications for low cost AUV development in the future, which is being examined further by colleagues [19]. The bathymetric change measurement technique is an important development as surf zone research is limited by a lack of repeatable bathymetry measurements in response to storm forcing. A sUXO embedded sensor package with both pressure (for measuring wave forcing and depth), light and orientation sensors was also optimized for sUXO applications. While this sensor does not have an IMU for high frequency orientation measurements, the combination of accelerometers and magnetometers allows an order of magnitude lower power consumption, thus longer endurance or smaller battery packs.

6. Literature Cited

1. Traykovski, P. and T. Austin, (2017), *Continuous Monitoring of Mobility, Burial and Re exposure of Underwater Munitions in Energetic Near Shore Environments*, https://apps.dtic.mil/dtic/tr/fulltext/u2/1029969.pdf, Editor., Woods Hole Oceanographic Institution Woods Hole United States.
2. Calantoni, J., T. Staples, and A. Sheremet, (2014), *Long Time Series Measurements of Munitions Mobility in the Wave-Current Boundary Layer*. US Naval Research Laboratory Stennis Space Center United States.
3. Shields, A., (1936), *Application of similarity principles and turbulence research to bed-load movement*. Soil Conservation Service.
4. Rennie, S.E., A. Brandt, and C.T. Friedrichs, (2016), *Initiation of motion and scour burial of objects underwater* Ocean Engineering (Submitted March, 2016).
5. Friedrichs, C.T., S.E. Rennie, and A. Brandt, (2016) *Self-burial of objects on sandy beds by scour: A synthesis of observations*, in *Scour and Erosion*, J. Harris and R. Whitehouse, Editors., CRC Press.
6. Catano-Lopera, Y.A. and M.H. García, (2007), *Geometry of scour hole around, and the influence of the angle of attack on the burial of finite cylinders under combined flows.* Ocean Engineering. **34**(5): p. 856-869.
7. Nielsen, P., (1992) *Coastal bottom boundary layers and sediment transport*. Vol. 4. World scientific.
8. Whitehouse, R., (1998) *Scour at marine structures: A manual for practical applications*. Thomas Telford.
9. Traykovski, P., (2007), *Observations of wave orbital scale ripples and a nonequilibrium time-dependent model.* Journal of Geophysical Research: Oceans. **112**(C6).
10. Meyer-Peter, E. and R. Müller. (1948), *Formulas for bed-load transport*. IAHR.
11. UXB International, I. (2014) *Remedial Investigation Report, Tisbury Great Pond Investigation Area, Martha's Vineyard, Massachusetts*. 2014; Available from: http://www.nae.usace.army.mil/Portals/74/docs/topics/MarthasVineyard/Tisbury/RemedialInvestigationReport.pdf.
12. Bruder, B.L., D. Cristaudo, and J.A. Puleo, (2016), *Observing Migration and Burial of Unexploded Ordnance in the Nearshore Environment with Instrumented Surrogates.* AGUFM. **2016**: p. OS32A-07.
13. Agisoft, L. and A.M.U. Manual, (2019), *Professional Edition, Version 1.5; Agisoft LLC: St.* Petersburg, Russia.
14. Jaffre, F., et al. (2015), *Development of underwater acoustic backscatter and Doppler instruments from a small and versatile multi-frequency sonar board with software defined processing*. in *OCEANS 2015-*. Genova: IEEE.
15. Moffet, A., (1968), *Minimum-redundancy linear arrays.* IEEE Transactions on antennas and propagation. **16**(2): p. 172-175.
16. Raghukumar, K., et al., (2019), *Performance characteristics of "Spotter," a newly developed real-time wave measurement buoy.* Journal of Atmospheric and Oceanic Technology. **36**(6): p. 1127-1141.
17. Zijlema, M., G. Stelling, and P. Smit, (2011), *SWASH: An operational public domain code for simulating wave fields and rapidly varied flows in coastal waters.* Coastal Engineering. **58**(10): p. 992-1012.

18. Rennie, S.E. and A. Brandt, (2015), *Underwater Munitions Expert System: Preliminary Design Report*. JOHNS HOPKINS UNIV LAUREL MD LAUREL.
19. Fischell, E.M., A.R. Kroo, and B.W. O'Neill, (2020), *Single-Hydrophone Low-Cost Underwater Vehicle Swarming.* IEEE Robotics and Automation Letters. **5**(2): p. 354-361.

7. Appendices

A. Supporting Data Table

a) sUXO Name	b) Migration Distance (m)	c) Freq (kHz)	d) L (m)	e) *D* (m)	f) S	g) r.m.s. pitch (°)	h) r.m.s. roll (°)	i) Mobility begin Ubr (m/s)	j) High Mobility Begin Ubr (m/s)	k) Mobility End Ubr (m/s)
LVLA	<5	39	0.75	0.1412	2.26	0.97	2.24	0.86	0.00	1.29
LLA	<5	32	0.75	0.1412	2.48	2.54	5.43	0.66	0.00	1.09
LMA	5.6	30	0.75	0.1412	2.78	3.47	50.34	0.85	1.08	1.34
LHA	<5	37	0.75	0.1412	3.02	1.92	1.99	0.59	0.00	1.14
LVLB	5.7	35	0.75	0.1412	2.25					
LLB	4.9	36	0.75	0.1412	2.46					
LMB	21.1	40	0.75	0.1412	2.75	1.59	55.57	0.49	1.48	1.38
LHB	6.3	34	0.75	0.1412	3.01					
SVLA	<5		0.75	0.0737	2.27					
SLA	<5		0.75	0.0737	2.54					
SMA	9.9	31	0.75	0.0737	2.65					
SHA	<5	38	0.75	0.0737	2.98					
SVLB	<5		0.75	0.0737	2.21					
SLB	<5		0.75	0.0737	2.52					
SMB	7.3		0.75	0.0737	2.65					
SHB	10.3	33	0.75	0.0737	2.98					

Table 1: Long Point surf zone object properties, migration, and Wave Velocity (U_{br}) statistics

Notes on table data:

Tables1 summarizes the migration of UXO deployed at Long Point Beach, Martha's Vineyard in 2018.

a. Object Names are grouped by the following:
   L series: Large diameter objects (some with MATPL sensors); VL for relative density S ~ 2.25, L for S ~ 2.5 , M for S ~ 2.75 , H for S ~ 3.0 , A and B are duplicate objects with similar properties
   S series: Small diameter objects with similar density descriptions.
b. Migration Distance (m). Migration distance under 5 m are within the measurement error.
c. Pinger acoustic frequency. Not all sUXO had pingers
d. Length (m)
e. Object Diameter (m)

f. Relative Density ($S_o = \frac{\rho_o}{\rho_w}$)
g. R.m.s. pitch variations during period of mobility
h. R.m.s. pitch variations during period of mobility
i. Wave velocity when small scale (< 5 °) roll variations begin
j. Wave velocity when large scale (>15°) roll variations begin
k. Wave velocity when roll variations end due to burial by the offshore migrating sandbar

Other data such as bathymetric data sets and hydrodynamic forcing time series are available from the lead investigator: ptraykovski@whoi.edu.

Technical Publications

a. Samuelson, K. *Migration of Multiple Scale Bedforms in Energetic Tidal Environments*. in *2016 Ocean Sciences*. 2016. New Orleans: AGU
b. Traykovski, P. *Phase lag control of tidally reversing mega-ripple geometry and bed stress in tidal inlets* in *2016 Ocean Sciences*. 2016. New Orleans: AGU
c. Traykovski, P. Observations of the Geometry and Migration of Tidally Reversing Dunes, Proceedings of Coastal Sediments, San Diego 2015